HHS Public Access

Author manuscript

Nat Neurosci. Author manuscript; available in PMC 2021 September 02.

Published in final edited form as:

Nat Neurosci. 2021 April ; 24(4): 478–488. doi:10.1038/s41593-020-00788-z.

Oligodendrocyte precursor cell specification is regulated by bidirectional neural progenitor–endothelial cell crosstalk

Isidora Paredes[1,2], **José Ricardo Vieira**[1,2], **Bhavin Shah**[1], **Carla F. Ramunno**[1,2], **Julia Dyckow**[3], **Heike Adler**[1], **Melanie Richter**[1], **Geza Schermann**[1], **Evangelia Giannakouri**[1,2,4], **Lucas Schirmer**[3,5,6], **Hellmut G. Augustin**[1,4], **Carmen Ruiz de Almodóvar**[1,6]

[1]European Center for Angioscience, Medical Faculty Mannheim, Heidelberg University, Mannheim, Germany.

[2]Faculty of Biosciences, Heidelberg University, Heidelberg, Germany.

[3]Department of Neurology, Medical Faculty Mannheim, Heidelberg University, Mannheim, Germany.

[4]Division of Vascular Oncology and Metastasis, German Cancer Research Center (DKFZ-ZMBH Alliance), Heidelberg, Germany.

[5]Mannheim Center for Translational Neuroscience and Institute for Innate Immunoscience, Medical Faculty Mannheim, Heidelberg University, Mannheim, Germany.

[6]Interdisciplinary Center for Neurosciences, Heidelberg University, Heidelberg, Germany.

Abstract

Neural-derived signals are crucial regulators of CNS vascularization. However, whether the vasculature responds to these signals by means of elongating and branching or in addition by building a feedback response to modulate neurodevelopmental processes remains unknown. In this study, we identified bidirectional crosstalk between the neural and the vascular compartment of the developing CNS required for oligodendrocyte precursor cell specification. Mechanistically, we show that neural progenitor cells (NPCs) express angiopoietin-1 (Ang1) and that this expression is regulated by Sonic hedgehog. We demonstrate that NPC-derived Ang1 signals to its receptor, Tie2, on endothelial cells to induce the production of transforming growth factor beta 1 (TGFβ1). Endothelial-derived TGFβ1, in turn, acts as an angiocrine molecule and signals back to NPCs to induce their commitment toward oligodendrocyte precursor cells. This work demonstrates

Corresponding author: carmen.ruizdealmodovar@medma.uni-heidelberg.de.

Author contributions

I.P. and C.R.d.A. designed the study and wrote the paper. C.R.d.A. supervised the study.
I.P. performed the experimental work and most of the data collection and analysis. J.R.V., B.S., C.F.R. and J.D. performed experiments and participated in data analysis. H.A.
and M.R. helped with the experiments and data analysis. E.G. helped by providing the Tie2 fl/flPdgfbCreERT2 mice. J.R.V. and G.S. performed bioinformatic analysis. I.P., C.R.d.A., J.R.V., B.S., C.F.R., J.D., L.S., H.G.A., E.G. and G.S. participated in data discussion and interpretation. All authors provided input and editing during manuscript preparation.
C.R.d.A. acquired the funding.

Competing interests

The authors declare no competing interests.

Extended data is available for this paper at https://doi.org/10.1038/s41593-020-00788-z.

Supplementary information is available for this paper at https://doi.org/10.1038/s41593-020-00788-z.

a true bidirectional collaboration between NPCs and the vasculature as a critical regulator of oligodendrogenesis.

Oligodendrocytes (OLs) arise from oligodendrocyte precursor cells (OPCs) and are the myelinating glial cells of the CNS. Impaired OL generation and function are key features of many diseases, such as multiple sclerosis in adults or periventricular leukomalacia, a typical dysmyelinating disorder in premature infants[1]. A better understanding of the mechanisms regulating OPC differentiation and maturation is, thus, essential for further defining strategies to treat such disorders.

Developmentally, OPCs derive from ventral NPCs in the motor neuron progenitor (pMN) domain as early as embryonic day 11.5 (E11.5) and start migrating into the mantle zone (MZ) from E12.5 in the mouse embryo[1,2]. Once specified, OPCs migrate away from their birth origin and proliferate to populate the entire CNS, upon which they undergo a process of terminal differentiation, becoming myelinating OLs[1,3]. However, a pool of OPCs (around 5% of all neural cells) do not mature into OLs during development but remain into adulthood in the parenchyma as immature cells that potentially act as a reservoir of OLs in case of disease or upon neural circuit requirement[3].

In the developing spinal cord (SC), most OPCs originate from the restricted Olig2-expressing pMN, which first gives rise to MNs and subsequently switches its fate to generate OPCs[2]. A second source of OPCs is generated later during development (at approximately E16.5) from dorsal progenitors and produces a minority of SC OPCs[3]. The pMN domain gives rise to the first wave of OPCs directed by the instructive morphogenic activity of floor plate-derived Sonic hedgehog (Shh)[2,4] and with Shh-mediated effects being regionally restricted by roof plate-derived bone morphogenetic proteins and Wnts[2]. Besides Shh, limited studies have addressed the potential contribution of other neural-derived signals in ventral OPC specification during development (for example, fibroblast growth factors (FGFs)[5], TGFβ[6,7] and Notch ligands Jagged and NB-3 (refs. [8,9])), raising the question of whether oligodendrogenesis requires additional signals (perhaps derived from other CNS compartments) that, together with Shh, cooperate to induce OPC commitment.

At the same time as NPCs proliferate and undergo differentiation, the CNS becomes vascularized[10]. Remarkably, blood vessels grow closely aligned to NPC domains without fully invading neurogenic areas[10,11]. By E12.5 in the developing mouse embryonic SC, at the time of OPC specification, vessels are in close proximity to the pMN domain[11]. Although CNS vascularization is known to be regulated by signals derived from the neural compartment and to acquire organ-specific properties[10], it is rather unknown whether the vasculature responds to these signals by just elongating and branching or whether they also build up a feedback response to signal back to the neural compartment. Moreover, the function that the developing vasculature might exert in NPCs during development, in particular during oligodendrogenesis, is largely unexplored.

Apart from performing their conventional function (transport of oxygen, nutrients, metabolites and cells), blood vessels are increasingly recognized as active orchestrators of organogenesis, tissue homeostasis and tissue regeneration[12-14]. Endothelial cell (EC)-

derived paracrine factors (also known as angiocrine), for example, can act on other cell types in their vicinity to influence their behavior. Different regulatory mechanisms, such as mechanical forces, hypoxia and activation of receptor tyrosine kinases pathways like vascular endothelial growth factor receptor 3 (ref. [15]) and Ang–Tie2 (ref. [16]), among others, have been linked to the production of angiocrine signals[12-14]. Angiopoietins are glycosylated proteins that bind to the tyrosine kinase receptor Tie2 (also known as TEK) in ECs to regulate EC survival, vessel stability and barrier function[12,17].

In this study, we identified a bi-directional NPC-to-EC molecular crosstalk, involving EC-derived angiocrine signaling, required for the precise timing of OPC specification during embryonic development. First, we discovered that Ang1 is expressed in NPCs and that its expression is regulated by Shh during embryonic development. We identified that NPCs actively communicate with the growing vasculature via the Ang1–Tie2 signaling axis and that this pathway is crucial for the production of EC-derived angiocrine TGFβ1, which then signals back to NPCs to promote their specification toward OPCs.

Results

Ang1 expression in the developing SC correlates with OPC specification.

In an attempt to better understand the expression of angiogenic factors in the developing mouse embryonic SC, we performed a temporal analysis of *Ang1* expression determined by in situ hybridization (ISH) (Fig. 1a and Extended Data Fig. 1a). Between stages E10.5 and E13.5, *Ang1* was expressed by ventricular NPCs and motor neurons (MNs) in a dynamic spatio-temporal manner (Fig. 1a and Extended Data Fig. 1a, b). At E10.5, *Ang1* was expressed by MNs (Isl1/2$^+$) (Extended Data Fig. 1b) and a ventral NPC domain (Fig. 1a). At E11.5, *Ang1* was expressed by several ventral progenitor domains, with the Olig2$^+$ pMN the most ventral progenitors expressing *Ang1* until at least E13.5 (Fig. 1a). The *Ang1* expression pattern was further confirmed by in silico analysis using previously published single-cell RNA sequencing datasets of all dorso-ventral SC progenitors between E9.5 and E13.5 (ref. 18) (Extended Data Fig. 1c). The expression pattern of *Ang1* led us to explore whether its expression in NPC domains could be regulating NPC behavior. Notably, the increase of *Ang1* transcript expression in ventral progenitors coincides with the process of OPC specification (Fig. 1b). Similarly to the SC, *Ang1* expression was also detected in the medial ganglionic eminence of the developing brain (Extended Data Fig. 1d), from where OPC specification also occurs beginning from E12.5. This expression analysis, together with the fact that Ang1 expression is not detected in a single-cell sequencing dataset of OPCs at different developmental stages (https://castelobranco.shinyapps.io/OPCsinglecell2017), indicated that Ang1 is not expressed (at detectable levels) in OPCs.

Altogether, we revealed a temporal correlation between OPC specification and *Ang1* expression during embryonic development, which prompted us to ask whether Ang1 itself could have a regulatory role in OPC generation.

Endogenous Ang1 expression is controlled by Shh and regulates OPC specification ex vivo.

One of the major regulators of OPC specification is Shh[4,19]. As Ang1 expression in astrocytes and fibroblasts is regulated by Shh[20,21], we questioned whether Shh could transcriptionally regulate *Ang1* expression in SC NPCs. For this, we isolated NPCs from E11.5 wild-type SCs and cultured them as neurospheres (NSPs) (Extended Data Fig. 2a-d). Consistent with the in vivo expression pattern, NSPs expressed *Shh* and *Ang1* under basal conditions (Extended Data Fig. 2d), and stimulation of NSP cultures with recombinant Shh resulted in an upregulation of Shh target gene encoding for patched 1 (*Ptch)* (Fig. 1c) as well as *Ang1* (Fig. 1d). *Ang1* expression was indeed dependent on Shh signaling as the addition of the Shh pathway inhibitor Sant1 (ref. [22]) abolished its induction (Fig. 1d).

To test the hypothesis that Ang1 signaling might regulate OPC development, we used ex vivo cultures of E11.5 mouse embryo SC explants (in an open-book preparation[23]), in which it is possible to analyze OPC specification and migration from the pMN domain to the MZ[24] (Extended Data Fig. 2e). To block endogenous Ang1, we treated the explants with a recombinant soluble Tie2 receptor (Tie2–Fc), which traps Ang1. Of note, OPCs ($Olig2^+$) migrating to the MZ after 24 h were reduced in Tie2–Fc-treated explants compared to vehicle-treated ones (Fig. 1e-g and Extended Data Fig. 2f). Sox10 is one of the earliest transcription factors expressed by pMN-NPCs in the ventricular zone (VZ) when committed to the OL lineage[1,3,25], and we found no accumulation of specified OPCs ($Olig2^+Sox10^+$ double-positive cells) in the pMN or its vicinity (Fig. 1e and Extended Data Fig. 2f), suggesting that migration of specified OPCs from the pMN was not affected. Notably, in the pMN, whereas similar numbers of $Olig2^+$ cells were seen, fewer $Sox10^+$ NPCs were observed (Fig. 1e), suggesting that Ang1 signaling from NPCs was required for OPC specification.

Finally, we asked whether Shh-regulated expression of Ang1 was required for Shh-mediated effects. Treatment of explants with Sant1 resulted in reduced OPC specification and downregulation of *Ang1* and *Ptch* (Extended Data Fig. 2g,h). OPC specification could be rescued by the addition of exogenous recombinant Ang1 (Extended Data Fig. 2g,i).

In summary, these results indicate that Ang1 expression in NPCs is regulated by Shh and that Ang1 is required (at least partially) for Shh-induced OPC specification ex vivo.

CNS-derived Ang1 regulates OPC specification in vivo.

Owing to early embryonic lethality of *Ang1* null embryos[26-28], we generated a CNS *Ang1* conditional knockout mouse line by crossing *Ang1* floxed mice (Ang1 fl/fl, kindly provided by Susan E. Quaggin[27]) with a Nestin:Cre driver line[29] that targets all neural progenitors (Fig. 2a), which showed *Cre* messenger RNA (mRNA) expression in SC NPCs as early as E11.0 (Extended Data Fig. 3a) and efficient Cre activity driven by Nestin at E11.5 (Extended Data Fig. 3b). Efficient deletion of *Ang1* mRNA in all NPCs in Ang1 $fl/fl^{Nestin:Cre}$ was already seen at E11.0 and E12.5 (Extended Data Fig. 3c,d). Embryos appeared normal in size (Extended Data Fig. 3e) and had normal Nestin expression pattern (Extended Data Fig. 3f), and the overall SC gross morphology at E12.5 remained unaffected (Extended

Data Fig. 3g,h). Using these embryos, we studied OPC specification by assessing the number of newly specified OPCs in the VZ and migrating OPCs localized in the MZ as previously reported[25]. At E12.5, *Ang1*-ablated embryos presented a strong reduction in OPCs ($Olig2^+Sox10^+$ double-positive cells) in the VZ and MZ at brachial (Fig. 2b,c and Supplementary Tables 1 and 2) and thoracic (Extended Data Fig. 3i,j and Supplementary Tables 3 and 4) levels. The total number of $Olig2^+$ cells in the pMN was similar between Ang1 fl/fl and Ang1 fl/fl$^{Nestin:Cre}$ animals (Fig. 2d and Extended Data Fig. 3k), resulting in a decreased ratio of VZ OPCs in Ang1 fl/fl$^{Nestin:Cre}$ embryos (Fig. 2e and Extended Data Fig. 3l). Consistently, ISH for *Pdgfra* (another commonly used OPC marker[3,30]) showed reduced OPC numbers in Ang1 fl/fl$^{Nestin:Cre}$ embryos compared to control littermates (Extended Data Fig. 3m). Altogether, this suggests that the reduced OPC number was due to a failure in OPC specification and not to a defect in cell death or proliferation of neural progenitors in general.

OPCs arise in the developing SC from the pMN domain ($Olig2^+$). As this domain was the most ventral NPC domain expressing Ang1 during SC development (Fig. 1a), we next asked whether the exclusive deletion of pMN-derived *Ang1* would also result in reduced OPC specification. Thus, we genetically deleted Ang1 in $Olig2^+$ pMN-NPCs by crossing Ang1 fl/fl with Olig2:Cre mice[31] (Fig. 2f). At E12.5, we detected mRNA expression of Olig2-driven *Cre* recombinase (Extended Data Fig. 4a), which resulted in an efficient deletion of *Ang1* in the pMN but not in the adjacent ventral domains of the developing SC (Extended Data Fig. 4b). The generated embryos developed normally and did not differ in size from control littermates, and the SC gross morphology was unaffected (Extended Data Fig. 4c-f). Similarly as in Ang1 fl/fl$^{Nestin:Cre}$, E12.5 Ang1 fl/fl$^{Olig2:Cre}$ embryos showed fewer OPC numbers in the MZ and in the VZ at brachial (Fig. 2g-j and Supplementary Tables 5 and 6) as well as at thoracic (Extended Data Fig. 4g-k and Supplementary Tables 7 and 8) levels.

To verify that the observed OPC reduction was specific to *Ang1* loss of function, we aimed to rescue the phenotype, using SC ex vivo explant cultures and applying exogenous recombinant Ang1. Similarly as observed in vivo, Ang1 fl/fl$^{Nestin:Cre}$ and Ang1 fl/fl$^{Olig2:Cre}$ resulted in reduced OPC counts in the MZ when compared to control littermates. Conversely, addition of exogenous Ang1 rescued the phenotype and increased the number of newly specified OPCs in Ang1 fl/fl$^{Nestin:Cre}$ and Ang1 fl/fl$^{Olig2:Cre}$ SC explants (Fig. 3a,b and Fig. 3c,d, respectively).

We then tested whether developmental myelination was altered in NPC-specific *Ang1*-deficient mice. To address this question, we analyzed the mRNA expression of *Plp* (encoding proteolipid protein (myelin) 1) and the protein level of myelin basic protein (MBP), the two major constituents of compact myelin[32]. Despite equal numbers of $Olig2^+$ cells at E16.5 (Extended Data Fig. 3n-o and Extended Data Fig. 4l-m), Ang1 fl/fl$^{Nestin:Cre}$ and Ang1 fl/fl$^{Olig2:Cre}$ embryos displayed reduced Plp^+ cell counts (based on ISH for *Plp* mRNA) (Extended Data Fig. 5a-d). Similarly, a reduced *Plp* expression pattern based on its density analysis was detected at P6 in Ang1 fl/fl$^{Nestin:Cre}$ (Extended Data Fig. 5e-h). However, Ang1 fl/fl$^{Olig2:Cre}$ did not show a difference in *Plp* expression at P6 (Extended Data Fig. 5i-l), probably due to compensation by *Ang1* expressed by other ($Olig2^-$) cell types. Next, we performed MBP staining and tissue clearing of thick slices of Ang1

fl/fl$^{Nestin:Cre}$ P6 SCs, followed by confocal deep imaging (Extended Data Fig. 5m) in high magnification. Using these image data and analyzing axonal and MBP staining over a distance/depth of 10–15 μm (see Methods for more details), we then quantified the percentage of myelinated axons (axons stained with neurofilament (NF) M antibody), MBP fluorescence intensity with respect to axon diameter, MBP-based myelin thickness and myelin thickness with respect to axon diameter (g-ratio). Although the number of axons and the percentage of myelinated axons were not altered in Ang1 fl/fl$^{Nestin:Cre}$ pups at P6 (Extended Data Fig. 5n-o), the overall MBP-myelin thickness showed a subtle reduction versus control littermates (Extended Data Fig. 5p). Notably, these data correlated with the reduction in myelin thickness and MBP intensity of large-caliber axons (g-ratio of axons larger than 0.8 μm in diameter) (Extended Data Fig. 5q-r). Overall, these results suggest that developmental myelination is impaired in the absence of Ang1 signaling.

Reduced OPC specification is not caused by differences in blood vessel density or hypoxia, nor by differential expression of Shh.

As the best known function of Ang1 is the regulation of blood vessel formation and maturation[17], we questioned whether the observed OPC specification defect could be a consequence of impaired vascularization. Although Ang1 fl/fl$^{Nestin:Cre}$ embryos presented a mild reduction in SC blood vessel density (Fig. 4a,b), Ang1 fl/fl$^{Olig2:Cre}$ did not reveal any difference (Fig. 4d,e). Moreover, no differences were observed in pericyte–blood vessel coverage in any *Ang1*-deficient embryos (Fig. 4c,f). Also, no functional defects were observed in any of the transgenic lines, as the expression of classical hypoxia-induced target genes (*Glut1*, *Vegfa*, *Bnip3*, *Egln3* and *Pdk1*) in the isolated neural compartment of E12.5 SCs was not different between *Ang1*-ablated embryos and their corresponding control littermates (Fig. 4g,h). The lack of hypoxia and the fact that no differences in blood vessel density were observed in Ang1 fl/fl$^{Olig2:Cre}$ embryos (whereas those embryos presented an OPC specification defect) suggest that the observed OPC specification defects were not a consequence of vascular malfunction. Also, OPC specification impairment could not be explained by differential expression of the main regulator, *Shh*, as its expression was not altered between Ang1 fl/fl$^{Nestin:Cre}$ or Ang1 fl/fl$^{Olig2:Cre}$ and their respective control littermates (Extended Data Fig. 6a-d).

Tie2 is exclusively expressed in blood vessels.

One potential mechanism of Ang1-mediated effects to regulate OPC specification could be that Ang1 signals directly to NPCs to induce specification. For this, Tie2, the cognate Ang1 receptor, should be expressed by NPCs. We analyzed *Tie2* expression in the developing SC by ISH from E11.5 to E13.5 and found that *Tie2* mRNA transcripts were detected only in blood vessel-like structures (Fig. 5a). Next, we used two different genetic approaches to confirm Tie2 localization to the endothelium: mTmG$^{Tie2:CreERT2}$, where *Tie2*-driven recombination leads to green fluorescent protein (GFP) expression, and Tie2:GFP mice[33]. In both cases, GFP signal was restrained to CD31^{+} ECs (Fig. 5b,c). Finally, Tie2 immunostaining also showed Tie2 expression confined to the vasculature (Fig. 5d). Consistently, *Tie2* mRNA was not detected in NSPs isolated from embryonic SCs (Extended Data Fig. 2d).

In line with the absence of Tie2 expression in NPCs and, thus, a lack of direct autocrine signaling of NPC-derived Ang1 to NPCs, in vitro OPC differentiation from SC NSPs was not altered with the addition of recombinant Ang1, nor by blockade of the endogenous ligand using Tie2–Fc (Extended Data Fig. 6e-g).

Endothelial Tie2 regulates OPC specification.

The above-mentioned results pointed toward a mechanism involving the vasculature, comprising Ang1 binding to EC–Tie2, and inducing a response in the vasculature. Therefore, we reasoned that, if Ang1 is activating Tie2 in blood vessels, its activation should be reduced in *Ang1*-deficient SCs. Consistent with this hypothesis, phospho-Tie2 (p-Tie2) signal was reduced in blood vessels in the ventral SC region of Ang1 fl/fl$^{Nestin:Cre}$ compared to control littermates (Fig. 5e).

Next, we tested the hypothesis that endothelial-derived cues triggered by Ang1–Tie2 signaling might promote OPC specification. For this, we analyzed OPCs in transgenic mouse embryos genetically lacking *Tie2* in ECs[34] (Tie2 fl/fl$^{Pdgfb:CreERT2}$) (Fig. 6a). To overcome early embryonic lethality, we induced *Tie2* deletion by tamoxifen delivery to pregnant females from E8.5 to E10.5 and analyzed embryos at E12.5 (Fig. 6b). Analysis of *Tie2* expression by ISH and by quantitative polymerase chain reaction (qPCR) in primary isolated ECs from embryonic SCs revealed that *Tie2* was efficiently deleted in Tie2 fl/fl$^{Pdgfb:CreERT2}$ embryos (Fig. 6c,d). At E12.5, *Tie2*-ablated embryos were alive and did not differ morphologically from control littermates (Extended Data Fig. 7a), consistent with a previous report[35]. Furthermore, deletion of *Tie2* in ECs from E8.5 did not cause severe vascular defects in the developing SC (Extended Data Fig. 7b-d).

Remarkably, Tie2 fl/fl$^{Pdgfb:CreERT2}$ embryos presented an OPC specification phenotype similar to the one observed in embryos in which *Ang1* was ablated from NPCs (Fig. 6e-h, Extended Data Fig. 7e-h and Supplementary Tables 9-12). Consistent also with the phenotype seen in NPC *Ang1*-deficient embryos, no accumulation of already specified OPCs in the pMN was observed in Tie2 fl/fl$^{Pdgfb:CreERT2}$ embryos (Fig. 6e), suggesting that migration of specified OPCs is not impaired. In addition, expression of the endothelial-derived chemokine (C-X-C motif) ligand 12 (Cxcl12) (previously shown to be implicated in the regulation of OPC migration along the vasculature[36]) in ECs isolated from SCs of Tie2 fl/fl$^{Pdgfb:CreERT2}$ embryos (or from SCs of Ang1 fl/fl$^{Nestin:Cre}$) was not altered compared to their corresponding control littermates (Extended Data Fig. 8a,b). These results, together with the observation of no accumulation of OPCs in the pMN vicinity, indicate that this regulatory step of OPC migration was not affected.

Altogether, these data indicate that Tie2 signaling in SC ECs is required for proper OPC specification. As blood vessel density was not affected, these data further highlight a potential angiocrine mechanism that could signal back to NPCs to induce OPC specification.

EC-derived TGFβ1 is regulated by Tie2 signaling and required for normal OPC specification.

Previous reports showed that TGFβ signaling is required during OPC development and CNS myelination. Notably, those reports were based on the deletion of TGFβ receptors in

NPCs, or its intracellular signaling effector SMAD3 (refs. [6,7,37]), without identifying and confirming the cellular source of the ligands. Consistent with previous studies[6,38], we found that, whereas *Tgfb2* (*Tgfβ2*) is expressed in the floor plate, MNs and SC NPC domains (Extended Data Fig. 8c,d), *Tgfb1* (*Tgfβ1*) is expressed in ECs at the developmental time points when OPC specification occurs (Fig. 7a). Similarly as in liver ECs, where Tie2 activation regulates *Tgfβ1* expression during liver regeneration[16], we found that *Tgfβ1* expression was upregulated in human brain microvascular ECs (HBMECs) and primary ECs isolated from SCs of E12.5 embryos upon activation of Ang1–Tie2 signaling (Fig. 7b,c). In line, blockade of the Tie2-induced intracellular signaling cascade by pharmacologically inhibiting the AKT/PI3K pathway with Ly294002 abolished the upregulation of *Tgfβ1* transcript upon Ang1 stimulation (Fig. 7d). Consistently, *Tgfβ1* expression was significantly reduced in ECs isolated from SCs of E12.5 Ang1 fl/fl$^{Nestin:Cre}$ and Tie2 fl/fl$^{Pdgfb:CreERT2}$ (Fig. 7e,f). By contrast, *Tgfβ2* was unaffected in the isolated neural compartment (CD31^{-} fraction) (Extended Data Fig. 8e,f).

We reasoned that, if EC-derived TGFβ1 is downstream of Ang1/Tie2 signaling, and it is required for OPC specification, its signalling should be decreased in NPCs of *Ang1*-deficient embryos. Indeed, quantitative analysis of the activation of the TGFβ1 intracellular effector SMAD3 (ref. [39]) in pMN cells showed reduced pSMAD3^{+}Olig2^{+} progenitors in Ang1 fl/fl$^{Nestin:Cre}$ embryos (Fig. 7g,h). Moreover, neutralization of endogenous TGFβ1 (using a functional TGFβ1-blocking antibody) in SC explants from wild-type embryos resulted in reduced OPC specification, suggesting that EC-derived TGFβ1 is required in this process (Fig. 7i). Consistently, recombinant TGFβ1, as compared to vehicle, could rescue the OPC specification phenotype using the SC explant culture system in both Ang1 fl/fl$^{Nestin:Cre}$ and Tie2 fl/fl$^{Pdgfb:CreERT2}$ genotypes (Fig. 7j,k).

Collectively, these results identify TGFβ1 as an EC-derived angiocrine signal, which is regulated by Ang1–Tie2 signaling, and that is required for proper OPC specification.

Discussion

This study identified a novel biological mechanism of intercellular communication between the neural and the vascular compartment of the developing CNS, required for normal oligodendrogenesis. Our data propose a novel collaborative model, in which neural cells and ECs take turns to instruct each other how to proceed to achieve the final goal of OPC specification (Extended Data Fig. 9). This involves: (1) signaling of floor plate-derived Shh to NPCs to regulate Ang1 expression; (2) NPC-derived Ang1 signals then to ECs, where it binds and activates Tie2 (3) to induce TGFβ1 expression (4); and then (5) EC-derived TGFβ1 acts as a paracrine cue that signals back to NPCs of the pMN domain and activates SMAD3 (6) to induce NPC commitment toward OPCs (7) (see proposed model in Extended Data Fig. 9).

To promote the OPC fate for pMN-NPCs, a temporal activation of Shh signaling in Olig2^{+} NPCs is essential[2]. Adjacent domains of progenitors or neighboring developing neurons respond to Shh signaling by expressing short-range factors, which, together with Shh, engage in the control of OPC specification[6,8,40]. Remarkably, here we show that Shh does

not only recruit the neural compartment to orchestrate its action but that it also engages the growing vasculature to control OPC specification, thus synchronizing both the nervous and the vascular system to achieve this goal. Shh does so in sequential steps. First, it induces Ang1 expression in NPCs so that Ang1 can then act on ECs to induce an angiocrine response (TGFβ1) that travels back to pMN-NPCs. Of note, *Ang1* or *Tie2* deletion in NPCs or ECs, respectively, does not lead to a complete loss of OPCs, suggesting that this crosstalk is required for proper OPC specification, but that, in their absence, other signaling pathways (for example, FGFs, Notch signaling, etc) are still able to induce OPC specification to some extent, or that other compensatory mechanisms could overcome the lack of Ang1–Tie2 signaling.

This study broadens the conventional view of Shh as a morphogen and includes the vasculature as an important mediator of Shh-induced effects for oligodendrocyte development. Recent evidence demonstrates that blood vessels are more than passive tubes, transporting gases, hormones and nutrients. Indeed, the vasculature is emerging as an active regulator of tissue formation, organ function and regeneration[12,14]. In this respect, a handful of reports show that EC-derived signals regulate neuronal migration, synaptic structure and plasticity, the docking of radial glial processes and the positioning of post-mitotic pyramidal neurons in the cerebral cortex[10,41,42]. Little is known, however, of the active role of the vasculature in instructing cell fate specification during CNS development. In this study, we show a functional active role for blood vessels in oligodendrogenesis. We found that activation of an EC angiocrine response (TGFβ1) is crucial for instructing pMN-NPCs to specify their fate toward OPCs. Although a role for TGFβ signaling in OPC specification in vivo has been proposed, those studies were based mainly on the OPC phenotype in SMAD3 full knockout embryos[7], in transgenic mice expressing a constitutive active form of TGFβ receptor I, or lacking TGFβ receptor I in NPCs[6], without focusing on the ligand source. Our data, thus, add further knowledge to this regulation, as we identified that ECs are a source of TGFβ1 and that this signaling is critical for OPC specification. As TGFβ1 is poorly diffusible[39], our data also suggest that ECs from growing blood vessels adjacent to the pMN would be perfectly located to supply TGFβ1 to this NPC domain.

Ang1 and *Tie2* null knockouts are embryonically lethal during mid-gestation due to failure in cardiac development, where angiocrine Ang signaling is necessary to regulate heart morphogenesis[28,43]. The analysis of the neural-specific Ang1 transgenic mouse lines generated in this study demonstrated that deletion of *Ang1* in the neural compartment, or in pMN-NPCs specifically, results neither in overall developmental abnormalities nor in severe vascular morphological or functional defects during SC development. Consistently, our data show that EC-specific deletion of Tie2 from E8.5 onward (via tamoxifen treatment and leading to approximately 75% *Tie2* reduction at E12.5 in SC ECs) did not show defects in blood vessel density in the developing SC, suggesting that, beyond E8.5, Ang1–Tie2 signaling might not be essential for blood vessel formation in the CNS. Whether vascular and morphological defects might appear at later stages of development remains to be investigated. Notably, SC ECs had reduced *Tgfβ1* expression, suggesting that, although blood vessels might be morphologically similar between control and transgenic embryos, their angiocrine profile is changed. *Ang1–Tie2* deletion in ECs leads to partial reduction of *Tgfβ1*, suggesting that *Tgfβ1* expression in ECs is also regulated by other molecular

mechanisms. This remaining expression of *Tgfβ1* could also be important for the remaining OPC specification observed in those mutants. These results, thus, highlight the role of Ang1–Tie2 signaling as a coordinator of the angiocrine response in ECs. Ang–Tie signaling is complex and context dependent, which comprises the activation of Tie2 not only via Ang1 but also via Ang2 (ref. [17]). Whether Ang2 participates in this identified crosstalk between NPCs and ECs requires further investigation.

CNS Ang1-deficient embryos presented OPC specification defects during embryonic development. Whether OPC numbers are later compensated by enhanced proliferation of the remaining committed OPCs, as described in the developing brain[44], requires further investigation. Although Ang1 fl/fl$^{Nestin:Cre}$ and Ang1 fl/fl$^{Olig2:Cre}$ presented reduced *Plp* expression at E16.5, at later developmental stages those differences remained evident only in Ang1 fl/fl$^{Nestin:Cre}$, suggesting that, in Ang1 fl/fl$^{Olig2:Cre}$ mice, the Ang1 that remains expressed in other progenitor domains is probably compensating. Interestingly, Ang1 fl/fl$^{Nestin:Cre}$ mice also presented mild alterations in early post-natal myelination of large-diameter axons, suggesting that there is a delay in the overall development of the OL lineage, and/or that a crosstalk between the vasculature and specified OPCs, via Ang1–Tie2 signaling (or indirectly via other factors regulated by Ang1 and/or Tie2), is necessary for differentiation and maturation of the oligodendrocyte lineage. Indeed, the latter possibility is supported by previous studies describing that, once specified, OPCs regulate post-natal angiogenesis[45] and that OPCs associate to the vasculature to migrate and colonize the entire CNS via EC-derived CXCL12 signaling to CXCR4-expressing OPCs[36]—thus, suggesting that, in those posterior events, the signaling might not be uni-directional (OPC to vessel or vessel to OPC) but, rather, bi-directional. Further analysis of myelin ultrastructure as well as deciphering the functional role of the vasculature (upon Ang–Tie2 activation) in OL differentiation and maturation is required to bring answers to these open questions.

In summary, this study integrated building blocks from different cellular compartments and describes a unique bi-directional crosstalk between the neural and the vascular compartment of the developing CNS, where those compartments coordinate with each other to converge into the instruction and control of oligodendrogenesis. Further elucidation of the mechanisms of intercellular communication between the vascular and the OL lineage will help to better understand the pathophysiological mechanisms of white matter disorders.

Methods

Animals.

All animal experiments, handling and care were approved by the Heidelberg University ethical committee and local animal welfare authorities (Regierungspräsidium Karlsruhe, Germany; references I19/13, G92/18, G47/16, T46/16, T36/17, T48/18 and T38/19) and in accordance with the National Institutes of Health (NIH) ‘Guide for the Care and Use of Laboratory Animals’. Generation of Ang1 floxed mice were described previously[27] and were kindly provided by Susan E. Quaggin. Ang1 floxed mice were crossed with previously described lines Nestin:Cre[29] (Ang1 fl/fl$^{Nestin:Cre}$, C57BL/6 background) or Olig2:Cre[31] (Ang1 fl/fl$^{Olig2:Cre}$, C57BL/6 background) to specifically delete the *Ang1* gene in all or in Olig2-neural progenitors, respectively. Ang1 fl/fl mice were used as controls.

Pups and adult Ang1 fl/fl$^{Nestin:Cre}$ were smaller than control (Ang1 fl/fl) littermates. However, they survived and generated a viable fertile progeny. Nestin reporter embryos were obtained by crossing Nestin:Cre mice with the ubiquitous Rosa26:mTomato-mGFP reporter (mTmG$^{Nestin:Cre}$, C57BL/6 background)[46]. Rosa26:mTomato-mGFP mice were obtained from Jackson Laboratories. Tie2 floxed mice[34] were crossed with Pdgfb:CreERT2-IRES-EGFP[47] mice to specifically delete Tie2 in the endothelium (Tie2 fl/fl$^{Pdgfb:CreERT2}$, C57BL/6 background). Tie2 fl/fl mice were used as controls. Embryonic Cre recombination was induced by oral administration of time-staged pregnant females with 2 mg per 30 g of body weight of tamoxifen (tamoxifen was prepared at a concentration of 10 mg ml^{-1} (prepared in peanut oil with 10% ethanol, which was evaporated after tamoxifen solubilization)). Tie2 reporter mice were obtained by crossing the Tie2:CreERT2 driver line[48] (kindly provided by Prof. M. Hecker) with the ubiquitous Rosa26:mTomato-mGFP (mTmG$^{Tie2:CreERT2}$, C57BL/6 background) reporter[46]. Embryonic Cre recombination was induced by intraperitoneal injections on time-staged pregnant females with 2 mg per 30 g of body weight of tamoxifen (10 mg ml^{-1}). The Tie2-GFP reporter mouse line was previously described[33] and obtained from Jackson Laboratories. Wild-type CD1 and C57Bl/6 mice were purchased from Janvier Labs and Charles River Laboratories.

Tissue processing.

Mouse embryos were collected at different embryonic stages (E9.5–E16.5) and fixed in 4% paraformaldehyde/PBS (DEPC treated) at 4 °C for 6–24 h depending on the embryonic stage. To study developmental myelination in neonates, P6 animals were perfused with 4% PFA, and SCs were dissected and post-fixed in 4% PFA at 4 °C overnight. Afterwards, embryos and post-natal SCs were cryoprotected with 30% sucrose/PBS-DEPC and subsequently embedded in OCT and stored at −20 °C. Cryosections were sliced in the transverse plane at 16-, 20- or 40-μm thickness using a cryostat (MICROM HM560). SCs used for clearing were kept in PBS until sectioning (see ‘SC clearing, immunostaining and imaging’).

Immunohistochemistry.

Frozen sections were washed, permeabilized and blocked in buffer solution containing 0.3% Triton X-100, 2% BSA and 2.5% normal donkey serum in PBS for 1 h and incubated with primary antibodies overnight at 4 °C. For immunofluorescence, the following primary antibodies were used at the indicated dilutions: mouse α-Isl1/2 (39.4D5, 1:200, DSHB), rabbit α-Olig2 (AB9610, 1:300, Millipore), mouse α-Olig2 (MABN50, 1:100, Millipore), rat α-PDGFRα (558774, BD Pharmingen), rabbit α-phospho Tie2 (AF2720, 1:100, R&D Systems), rat α-Tie2 (16-587-82, 1:50, eBioscience), rabbit α-phospho SMAD3 (ab52903, 1:100, Abcam), goat α-Sox10 (AF2864, 1:300, R&D Systems), rat α-CD31 (557355, 1:100, BD Pharmingen), chicken α-Nestin (NES, 1:1000, Aves), rabbit α-NG2 (AB5320, 1:100, Millipore), rabbit α-GFP (A11122, 1:100, Invitrogen), rat α-MBP (MCA409S, 1:500, AbD Serotec), rabbit α-Neurofilament-M (1:800, 841001, BioLegend) and mouse α-Neurofilament-M 2H3 (1:50, AB_2314897, DSHB). The secondary antibodies were incubated for 2 h at room temperature. The conjugated secondary antibodies used were as follows: donkey α-mouse Alexa405 (175658, Abcam), donkey α-mouse Alexa488 (715-545-150, Jackson ImmunoResearch), donkey α-goat Alexa488 (705-545-003, Jackson

ImmunoResearch), goat α-chickenA488 (A11039, Molecular Probes), donkey α-rabbit Alexa488 (711-545-152, Jackson ImmunoResearch), donkey α-rabbitA568 (A10042, Molecular Probes), donkey α-rabbit Alexa647 (711-605-152, Jackson ImmunoResearch) and goat α-mouse Isotype IgG2b-A568 (A21144, Invitrogen). All secondary antibodies were used at a concentration of 1:500. Blood vessels were visualized using Isolectin GS-IB_4 Alexa Fluor 568 conjugate (I21412, 1:250, Invitrogen). Images were collected on a confocal microscope (Zeiss LSM 510 unit mounted on an Axiovert 200 M inverted microscope or Zeiss LSM800) with ×20/0.8 Plan-APOCHROMAT or ×40 Plan-APOCHROMAT and on a Nikon AR1 confocal microscope with ×20/0.75 and ×40/1.3 Plan-Fluor Objective. Image processing was performed using NIH ImageJ software.

Whole-mount vibratome sections were used for analyzing blood vessel density and pericyte coverage. Immunostainings were performed as previously described with modifications[49]. Briefly, PFA-fixed E12.5 embryos were embedded in 5.5% agarose and sectioned at 100-μm thickness on a vibratome (Leica VT1200S). Then, the sections were permeabilized for 1 h in PBS-T (PBS with 1% Triton X-100) and afterwards blocked for 4 h at 4 °C in 2.5% normal donkey serum and 1% BSA in PBS. Subsequently, the sections were incubated with primary antibodies diluted in blocking buffer overnight at room temperature. Primary antibody was washed with PBS five times for 20 min and incubated with secondary antibodies and Isolectin GS-IB_4 Alexa Fluor 568 conjugate diluted in blocking solution overnight at 4 °C. Finally, sections were washed five times for 20 min at room temperature with PBS and mounted. Images were acquired on a Nikon A1R confocal microscope.

ISH.

For detection of mRNA expression, ISH was performed using the following riboprobes: *Ang*1 and *Tie*2 (gift from H. Marti), *Shh* (gift from P. Carmeliet), *Cre* (using the following primers: forward: 5′-ACCAGGTTCGTTCACTCATGG-3′ reverse: 5′-AGGCTAAGTGCCTTCTCTACAC-3′), *Plp*, *Pdgfra*, *Tgfβ1* and *Tgfβ2* (using the primer sequences provided in the Allen Brain Atlas). Briefly, digoxigenin (DIG)-labeled antisense riboprobes were used on frozen sections to hybridize overnight between 68° and 72 °C. DIG riboprobes were detected with alkaline phosphatase-conjugated anti-DIG antibody (1:2,000, Roche Diagnostics) and developed with nitroblue tetrazolium (Promega) and 5-bromo-4-chloro-3-indolyl phosphate (Promega), which formed a violet precipitate between 1 and 48 h. In parallel, as negative control, sections were incubated with sense DIG-labeled riboprobes that gave no specific signal. Stainings were imaged under a Zeiss Axiovert 200 fluorescence microscope equipped with an AxioCam MRc camera.

Combined ISH and immunofluorescence.

Frozen sections were processed with the regular ISH protocol as described above. After color development, sections were post-fixed with 4% PFA for 20 min. Subsequently, samples were rinsed in PBS and processed for immunofluorescence. Sections were first permeabilized and blocked with 2% BSA and 0.3% Triton X-100 in PBS solution for 1 h. Incubation of primary antibodies was carried out for 48 h at 4 °C. Samples were washed five times for 10 min with PBS and incubated with secondary antibodies for 24 h at 4 °C. Finally, sections were washed and mounted for imaging.

SC explant culture and processing.

SCs from E11.5 embryos were processed for explant culture as previously described with minor modifications[24]. Briefly, SCs were dissected on L15 medium containing 5% horse serum, 50 U ml^{-1} of penicillin and 50 μg ml^{-1} of streptomycin via open-book preparation[23]. Subsequently, isolated SCs were flat mounted on cell culture inserts (PICM01250, Millipore) with neural progenitors facing upwards. Explants were maintained as organotypic cultures in air–medium interface using DMEM (Sigma-Aldrich) supplemented with 10% FBS (S0115, Biochrom), 100 U ml^{-1} of penicillin and 100 μg ml^{-1} of streptomycin. As soon as the explants were mounted, they were cultured with or without Tie2–Fc 2 μg ml^{-1} (762-T2-100, R&D Systems), Sant1 300 nM (559303, Calbiochem), Ang1 300 ng ml^{-1} (923-AN, R&D Systems), TGFβ1 50 ng ml^{-1} (7666-MB-005, R&D Systems), chicken α-TGFβ1/1.2 blocking antibody 5 μg ml^{-1} (AF-101-NA, R&D Systems) or chicken IgY isotype control (AB101, R&D Systems) for 24 h and then either lysed for RNA extraction or fixed in 4% PFA for immunohistochemistry. Explants were sectioned at a 100-μm thickness using a tissue chopper (McIlwain) and imaged on a Zeiss LSM 510 confocal microscope or a Zeiss LSM 800 inverted microscope with ×20/0.8 Plan-APOCHROMAT or on a Nikon AR1 confocal microscope with ×20/0.75 Plan-Fluor Objective. Image processing was performed using NIH ImageJ software.

OPC quantification.

The number of OPCs was determined in 16–18-μm cryosections at brachial or thoracic SC levels at E12.5 and E16.5 and in 100-μm sections of SC explants. The total number of OPCs was obtained by counting $Sox10^{+}Olig2^{+}$ double-positive cells in the VZ and by counting $Olig2^{+}$ cells in the MZ, per section in at least five sections per embryo. The obtained results were normalized to the respective control littermates. The percentage of newly born OPCs in the VZ was calculated by determining the number of $Sox10^{+}$ cells over the total number of $Olig2^{+}$ pMN progenitors in the VZ. Quantification was done blinded to the experimental condition.

Image analysis of blood vessel density and pericyte coverage.

Quantification of blood vessel density and pericyte analysis was performed using NIH Image J software by automated quantification. The ratio of the SC area covered by blood vessels (blood vessel density) was calculated as the area covered by $IsoB4^{+}$ staining per SC cross-section area, obtaining the percentage blood vessels in the SC. The obtained results were normalized to the respective control littermates (normalized blood vessel area). Images of SC cross-sections were projected as Z-stacks with the maximum intensity and processed as binary 8-bit pictures applying the Enhance contrast (saturated pixels 0.4% selecting normalization equalization), Despeckle, Gaussian blur (sigma = 1) filters and finally running background subtraction (rolling ball radius = 30 pixels) to remove noise and smoothen edges. Afterwards, a mask was created that was set for automatic threshold (minimum value 37 pixels, maximum value 255 pixels) and a final mask generated from which the vessel area was analyzed using the particle analyzer function.

Relative pericyte coverage was analyzed by measuring the $NG2^{+}$ density area and obtaining a percentage of this value over the blood vessel density area of the same section/image.

Pericyte density was obtained by first producing a pixel-based segmentation of $NG2^+$ staining using the 'Trainable Weka Segmentation' function. Afterwards, a mask was created that was processed by applying the Despeckle, Gaussian blur (sigma = 1) filters. Next, the images were automatically thresholded and pericyte density calculated using the particle analyzer function. Only particles larger than 10 pixels were considered for the analysis. Pericyte coverage relative values were plotted, meaning that single values per mouse were normalized to the average of the wild-type littermates (Norm. pericyte coverage).

For each experiment, at least five cross-sections were analyzed per embryo from at least three independent litters. Quantification was done blinded to the experimental condition.

Image analysis of Ang1 expression by ISH and correlation to OPC numbers.

In Fig.1b, we plotted the relationship between OPC specification and Ang1 expression in ventral progenitor domains from E9.5 to E13.5. OPC numbers in the pMN (OPC counts: $Sox10^+Olig2^+$ double-positive cells) were plotted in the right *y* axis and Ang1 expression (%) in the left *y* axis. For *Ang1* expression, *Ang1* signal was quantified from ISH images based on the percentage of Ang1-positive signal area in the ventral NPC domains of the SC (*Ang1* expression (%)) selected as the region of interest (ROI) using NIH ImageJ software.

Image analysis of *Plp* ISH.

Plp-stained 18-μm P6 cross-sections were analyzed to obtain the density of *Plp*-stained surface area in the SC. Briefly, the whole SC or the ventral white matter was selected as the ROI. Next, all pictures were processed equally as binary 8-bit images and directly thresholded for gray matter, ventral white matter and whole SC analysis. Afterwards, a mask was created that was analyzed using the Analyze particles function and considered for the analysis only particles larger than 10 pixels. Finally, the Area% within the ROI, which represented the surface area stained with *Plp* (%*Plp* density), was obtained and plotted.

SC clearing, immunostaining and imaging.

Based on previously published clearing protocols[49], 4% PFA-perfused and post-fixed P6 SCs from control or mutant littermates were embedded in 5% low-melting agarose and cut on a vibratome cross sectionally to obtain 500-μm slices. The slices were washed in PBS three times and then stained and cleared using a modified BABB clearing protocol[49]. In brief, the slices were bleached in Dent's bleach (1 part H_2O_2 + 2 parts Dent's fixative) overnight at 4 °C with shaking. After this, the slices were washed in methanol five times (10 min each) and fixed in Dent's fixative (20% DMSO + 80% methanol) and incubated overnight at 4 °C with shaking. SC slices were then washed three times with PBS (15 min each) and blocked in blocking buffer (20% DMSO, 5% normal donkey serum, 75% PBST (PBS with 0.5% Triton X-100) and 0.025% sodium azide) for 2 h. Slices were then incubated in primary antibodies prepared in blocking buffer for 3 d at 35 °C with shaking. After five washes of 30 min each in PBST, the slices were subjected with Alexa Fluor-conjugated secondary antibodies (prepared in blocking buffer) and incubated for 48 h at 35 °C with shaking for 1 d. Next, the slices were washed with PBST five times (30 min each), and the final wash was replaced with 50% methanol (50% methanol + 50% PBST). After two more washes with only methanol (to dehydrate), the final wash in methanol was

replaced by 50% BABB solution (50% methanol + 50% BABB) (1 part benzyl alcohol and 2 parts benzyl benzoate). After a 5-min wash, the slices were changed into 100% BABB solution, and they immediately became transparent and were stored in fresh BABB solution until further use (4 °C). The ventral funiculus area was imaged for NF and MBP on a ×63 objective (NA-1.4-3x zoom) using a Zeiss LSM800 microscope setup with 0.5-μm step size. Imaging was possible up to a maximum depth of 60–70 μm, which was then used for three-dimensional reconstruction using IMARIS software (version 9.5.1) or image analysis of single slices using NIH ImageJ software.

Analysis of myelin in thick SC slices.

For determining MBP-based myelin thickness or g-ratio (a measure of myelin thickness with respect to the axon diameter), MBP-positive stained rings enclosing NF^+ axons were randomly selected and manually measured. Assuming a consistent thickness of axon fiber and MBP coverage over a distance of 10–15 μm, each neuronal axon (and surrounding MBP-positive myelin ring) was measured three times (in three measurements: start, 0 μm; middle, 5–7 μm; and end, 10–15 μm) and averaged. To obtain the average axon diameter and fiber diameter (MBP ring + axon diameter), a line segment was drawn covering the NF^+ diameter and MBP ring + NF^+ diameter, respectively, using ImageJ measurement tools. Myelin thickness was calculated as ([fiber diameter − axon diameter]/2), and g-ratio was calculated as (axon diameter/fiber diameter). Percentage of myelinated axons was determined by calculating manually the number of myelinated axons (NF^+ axons surrounded by MBP) with respect to the total number of axons (NF^+) in a field of view. The fluorescence intensity of MBP rings was measured by manually selecting MBP ring area as an ROI or selecting a background area of transformed 8-bit images and calculating the corrected fluorescence intensity (CFI) by measuring the area of integrated intensity and the mean gray value as (CFI = integrated density−[area ROI × mean fluorescence of background]). A minimum of ten axons were measured per slice image, and four image stacks per mouse were collected. The analysis was performed with five Cre+ and four Cre^- animals and blinded to the experimental condition.

EC isolation from embryonic ECs.

SC tissues from BL6 E12.5 mouse embryos were dissected on L15 medium containing 5% horse serum, 50 U ml^{-1} of penicillin and 50 μg ml^{-1} of streptomycin via open-book preparation[23] and dissociated after 10-min incubation with 0.05% trypsin and DNAse 10 ug ml^{-1}. Afterwards, the endothelial compartment was enriched by sorting $CD31^+$ cells using magnetic mouse CD31 MicroBeads (130-097-418, MACS Milteny Biotec) in combination with MS Columns (130-042-201, MACS Milteny Biotec) following the manufacturer's instructions. The neural compartment was collected by negative selection from the $CD31^-$ fraction.

Cell culture.

HBMECs (Cell Systems) and primary SC ECs sorted after MACS enrichment were cultured in well plates coated with 0.1% gelatine in Endopan 3 complete medium for ECs (PAN-Biotech) supplemented with 10% FBS, 100 U ml^{-1} of penicillin and 100 μg ml^{-1} of streptomycin (both Gibco by Life Technologies) in a 5% CO_2 humidified incubator at 37 °C.

HBMECS from passages 6 to 10 were used for the experiments. HBMECS and primary SC ECs were starved in growth factor-free Endopan 3 supplemented with 2% FBS, 100 U ml^{-1} of penicillin and 100 μg ml^{-1} of streptomycin before stimulation with recombinant Ang1 300 ng ml^{-1} (923-AN, R&D systems), Ly294002 (440202, Calbiochem) 40 μM or vehicle. After 24 h, cells were lysed for RNA extraction.

Neurosphere culture.

E11.5 wild-type CD1 embryos were dissected to isolate the SC via open-book preparation[23]. SCs were dissociated after 10-min incubation with 0.05% trypsin and DNAse 10 μg ml^{-1} (LS002139, Worthington) to a single-cell suspension. Afterwards, cells were maintained in DMEM/F12 (Sigma-Aldrich) supplemented with 6 mg ml^{-1} of glucose (G8644, Sigma-Aldrich), non-essential amino acid mixture (Sigma-Aldrich, M7145), pyruvate (Sigma-Aldrich, S8636), B27 (17504044, Gibco), N2 (17502048, Gibco), 10 ng ml^{-1} of EGF (2028-EG, R&D Systems), FGF-2 20 ng ml^{-1},100 U ml^{-1} of penicillin and 100 μg ml^{-1} of streptomycin. The cells were allowed to form spheres for 7–10 d, and half of the medium was replenished every 3–4 d. For the experiments, and to obtain a larger number of cells, the primary NSPs (NSP-1) were passaged and gently dissociated to single cells and cultured for another 5–7 d in the same conditions. Secondary NSPs (NSP-2) that grew in suspension were stimulated with recombinant Shh 500 ng ml^{-1} (923-AN, R&D Systems) and/or Sant1 150 nM (559303, Calbiochem) and lysed for RNA extraction.

To differentiate NSP-derived neural progenitors, secondary NSPs were plated on 0.02 mg ml^{-1} of poly-L-lysine-coated coverslips (P1524, Sigma-Aldrich) in DMEM/F12 (Sigma-Aldrich) medium containing 6 mg ml^{-1} of glucose (G8644, Sigma-Aldrich), non-essential amino acid mixture (Sigma-Aldrich, M7145), pyruvate (Sigma-Aldrich, S8636), N2, B27, 100 U ml^{-1} of penicillin and 100 μg ml^{-1} of streptomycin and stimulated with recombinant Ang1 100 ng ml^{-1} (923-AN, R&D Systems) and/or Tie2–Fc 2 μg ml^{-1} (762-T2-100, R&D Systems). Differentiated cells were fixed for 20 min with 4% PFA and processed for immunocytochemistry.

RNA extraction, conventional and qPCR.

RNA from tissue and cultures was extracted using the RNeasy Mini Kit (Qiagen, 74104). RNA from primary ECs was extracted using the RNeasy Micro Kit (Qiagen, 74004). Polyadenylated RNA samples were DNAseI treated (EN0521, Thermo Fisher Scientific) and reverse transcribed to complementary DNA using either Maxima Reverse Transcriptase (EP0742, Thermo Fisher Scientific) or SuperScript Vilo (11754-050, Thermo Fisher Scientific) following the manufacturer's protocols. Conventional PCR was performed with NSP-extracted mRNA. PCR parameters were adjusted for each set of primers using Taq polymerase for the reactions (Sigma-Aldrich, D4545-1.5KU). The amplification protocol was adjusted according to primers listed in Supplementary Table 13. The obtained products were resolved in 2% agarose gels. Quantitative real-time PCR products were detected on a StepOn Real-Time PCR system (Thermo Fisher Scientific) performed using Fast SYBR Green Master Mix (00408995, Thermo Fisher Scientific). *Gapdh* or *β-actin* transcripts were used as endogenous controls for normalizing the relative expression level of target genes

(Supplementary Table 14). All qPCR results were obtained from at least three biological repeats.

In silico analysis of Ang1 expression.

Plotting Ang1 expression was performed using previously published single-cell RNA sequencing data from the embryonic SC at different developmental stages[18]. The available single-cell RNA sequencing data were downloaded from ArrayExpress (accession number E-MTAB-7320) and analyzed using R (version 3.6.1; http://www.R-project.org/). The dataset was analyzed using the pipeline published by Delile et al.[18] for the Mouse Spinal Cord Atlas (https://github.com/juliendelile/MouseSpinalCordAtlas) with minor changes: for the plot of *Ang1* expression (Extended Data Fig. 1c), the background correction was modified from the original pipeline, setting a threshold that considered positive *Ang1* expression if at least two cells of a particular domain express more than one *Ang1* transcript.

Statistical analysis.

All data bar plots are expressed as the mean for each group, and all include two-sided error bars that represent ± s.e.m. of at least three biologically independent experiments. To calculate the statistical significance of differences between two groups, a parametric unpaired Student's *t*-test or non-parametric Mann–Whitney U-test was used if applicable. One-way analysis of variance (ANOVA) followed by Sidak's multiple comparisons was used to determine the statistical significances of three or four groups. Two-way ANOVA followed by Sidak's multiple comparisons test was performed to determine the statistical significance among four groups that were categorized on two independent variables. Data distribution was assumed to follow a normal distribution (but was not formally tested). Statistically significant results are indicated in the figures using $*P < 0.05$, $**P < 0.01$ $***P < 0.001$ and $****P < 0.0001$. Sample sizes were determined according to previous publications where at least three animals per genotype or condition were analyzed[10,25], and no statistical method was used to predetermine sample sizes. In embryo or pup experiments, randomization was not applicable corresponding to the analysis of Cre^- versus Cre^+ animals stained with the same antibodies or ISH probes. For explant experiments, mouse embryos were randomly assigned for the different stimulations. Analysis was performed blinded to the experimental conditions. Statistically significant outlier data points were removed. The statistical analysis was performed using GraphPad Prism (version 6.0) (GraphPad Software). See Source Data for statistical parameters of all data presented.

Reporting Summary

Further information on research design is available in the Nature Research Reporting Summary linked to this article.

Data availability

The data that support the findings of this study are available in the manuscript or the Supplementary Information. All reagents and additional data from this study are available upon reasonable request from the corresponding author. Source data are provided with this paper.

Code availability

The modifications to the original code of Delile et al.[18] are available upon reasonable request. Source data are provided with this paper.

Extended Data

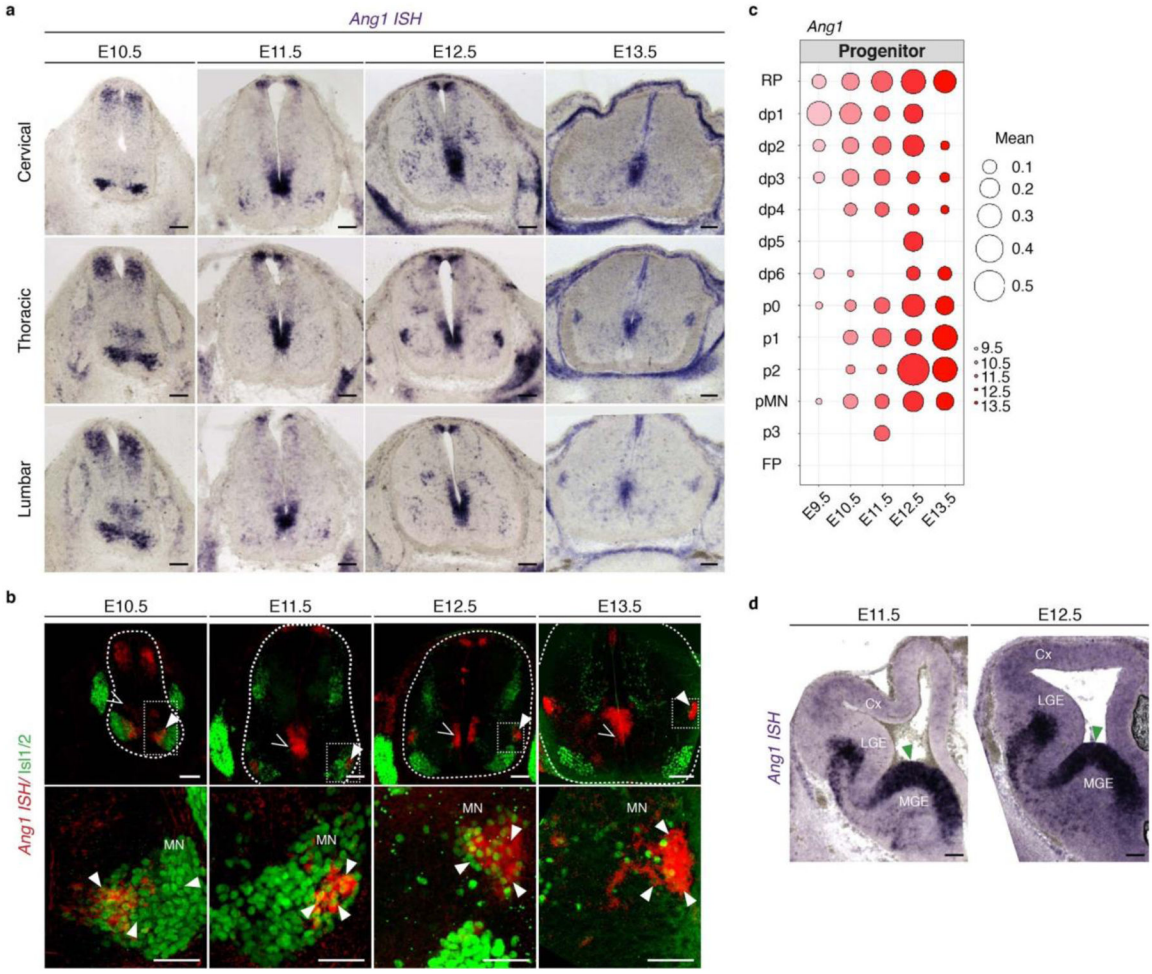

Extended Data Fig. 1 |. Ang1 is dynamically expressed in the embryonic developing SC and forebrain.

a, *ISH* for *Ang1* in transverse sections from E10.5 to E13.5 in the anterior-posterior axis of the SC (cervical, thoracic and lumbar levels). Data is representative from at least 3 independent experiments. Scale bar 100μm. **b**, Combined *Ang1 ISH* (pseudo-coloured in red) with immunofluorescence for Isl1/2^{+} motor neurons (green). At E11.5 *Ang1* is expressed only in a subset of brachial and lumbar motor neurons. At E12.5 and E13.5 *Ang1* is expressed by a dorsal-thoracic MN population. Data is representative from at least 3 independent experiments. Scale bar 50μm (inset) and 100μm (upper panel). Open arrowhead points to *Ang1* expression in NPCs. Filled arrowhead points to MN expressing *Ang1*. MN: motor neuron. **c**, Predicted expression of *Ang1* in all neural progenitors between E9.5 to E13.5 using previously published single-cell RNAseq data[18]. Ang1 is continuously expressed in a group of ventral progenitor domains (pMN-p0) from E10.5 to E13.5, while its

expression is continuously decreased in a group of dorsal progenitors (dp2-RP) from E9.5 to E13.5. A threshold considering that *Ang1* was expressed if at least two cells of a particular domain express more than one *Ang1* transcript was set to show *Ang1* positive expression. **d**, *Ang1 ISH* in forebrain coronal hemi-section detected at E11.5 and E12.5. Green arrowhead points to *Ang1* expression in the MGE. Data is representative from at least 3 independent experiments. Scale bar 100 μm. Cx: cortex. LGE: lateral ganglionic eminence. MGE: medial ganglionic eminence.

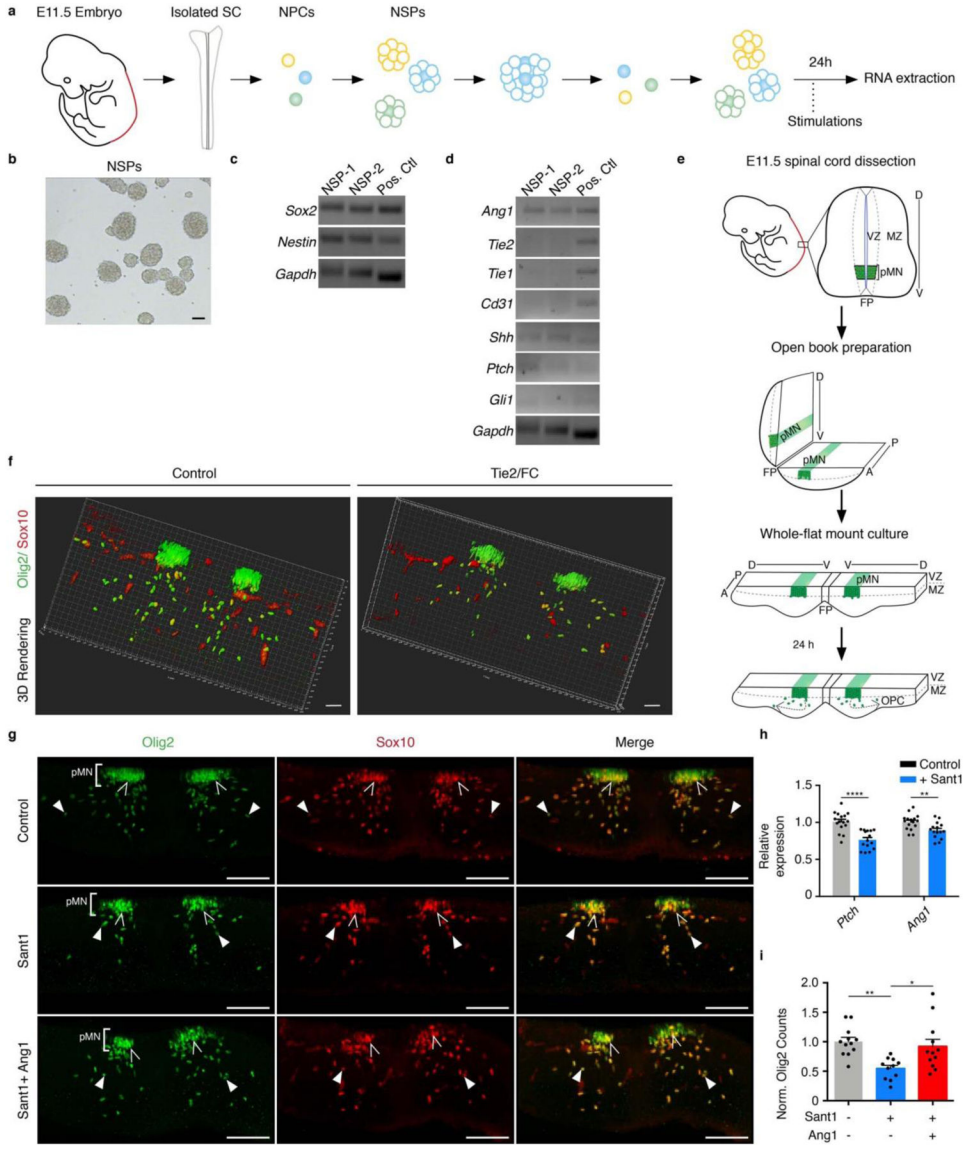

Extended Data Fig. 2 |. Shh-induced Ang1 is required for OPC specification.

a, Scheme showing the steps to obtain neural progenitor-derived neurospheres (NSPs) from a single-cell suspension collected from E11.5 SCs via ‘open book preparation’. After the second passage NSPs were stimulated for RNA extraction. **b**, Image of Secondary NSPs (NSP-2) used for all experiments. Data is representative from at least 3 independent experiments. Scale bar 100μm. **c**,**d**, NSPs (in first (NSP-1) or second passage (NSP-2))

express characteristic neural stem cell markers such as *Sox2* and *Nestin* (**c**). NSPs express components of the Shh pathway (*Shh, Ptch* and *Gli1*), *Ang1*, but not its receptor *Tie2*, its co-receptor *Tie1* nor the endothelial cell marker *Cd31* (**d**). Data is representative from 3 independent experiments. **e**, Scheme illustrating the steps for preparation of flat-mount SC explants. The SC of E11.5 embryos was isolated by 'open book preparation'. SC 'open books' were cultured for 24 h. The dashed line indicates the limit of the ventricular zone (VZ) and the mantle zone (MZ). V: ventral; D: dorsal; A: anterior; P: posterior. FP: floor plate. pMN: motor neuron progenitor domain. **f**, Example of 3D rendering of explants images (images are shown in 2D in main Fig. 1e). Scale bar 50μm. **g**, Transverse sections of wild-type SCs explants immunostained for Olig2 and Sox10 to detect OPCs in the VZ (open arrowheads) and MZ (filled arrowheads) after culturing with vehicle (control DMSO), Shh inhibitor Sant1 300 nM, and/or Ang1 300 ng/mL for 24 hours. Scale bar 100 μm. **h**,**i**, Relative expression of *Ptch* (**h**) and *Ang1* (**i**) mRNA of control (vehicle) and Sant1 treated wild-type SC explants. Graphs show mean±SEM (Control n = 16, Sant1 n = 15 of 4 independent litters). Unpaired two-sided T-Test, *Ptch* ****p<0.0001, Ang1**p=0.0062. **j**, Quantification of the number of OPCs in the MZ of the different conditions shown in (**g**), normalized to control. Graph show mean±SEM (Control n = 12, Sant1 n = 11, Sant1+Ang1 n = 12, of 5 independent litters). One-way ANOVA, Control vs +Sant1 **p=0.0027; +Sant1 vs +Sant1+Ang1 *p=0.0155.

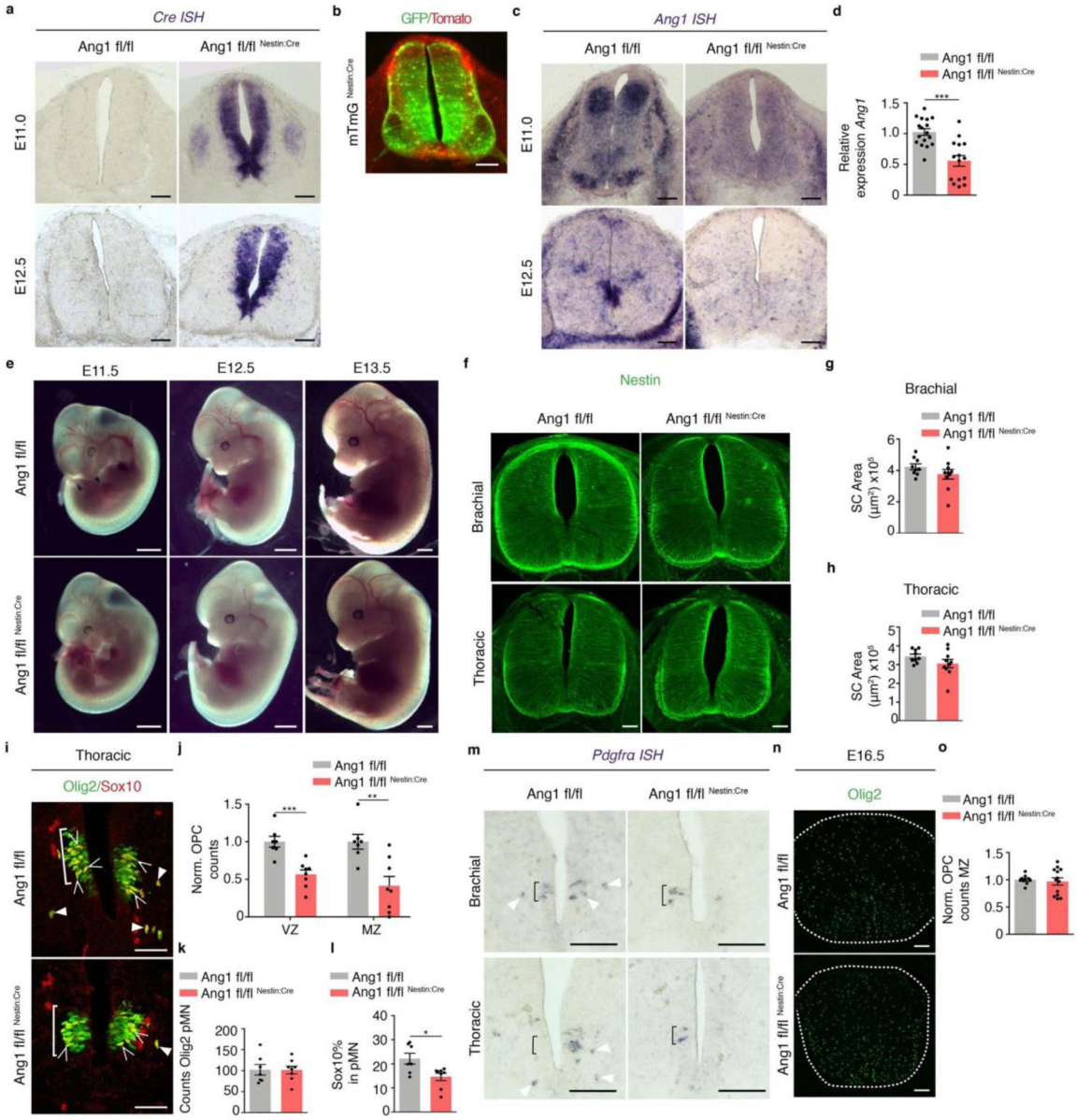

Extended Data Fig. 3 |. Ang1 fl/fl$^{Nestin:Cre}$ embryos and SC gross morphology appear normal, but show OPC specification defects.

a, *ISH* for *Cre recombinase* in transverse sections of E11.0 and E12.5 Ang1 fl/fl and Ang1 fl/fl$^{Nestin:Cre}$ embryo showing Cre expression. Data is representative from 3 independent embryos per genotype, from 2 litters. Scale bar 100µm. **b**, Transverse section of mTmG$^{Nestin:Cre}$ E11.5 reporter embryo, showing Nestin-driven recombination, and consequently GFP expression (green), in NPCs and differentiated cells. Tomato (red) is excluded from Nestin expressing tissue. Data is representative from 3 independent embryos from one litter. Scale bar 100 µm. **c**, *ISH* for *Ang1* in transverse sections of E11.0 and E12.5 Ang1 fl/fl and Ang1 fl/fl$^{Nestin:Cre}$ embryo showing efficient deletion of *Ang1* mRNA in Ang1 fl/fl$^{Nestin:Cre}$ embryos. Data is representative 3 independent embryos per genotype, from 2 litters. Scale bar 100µm. **d**, Relative *Ang1* mRNA expression in the

neural compartment ($CD31^-$ negative fraction from $CD31^+$ MACS isolation) from Ang1 fl/fl and Ang1 fl/fl$^{Nestin:Cre}$ E12.5 SCs. Graph show mean±SEM (Ang1 fl/fl n = 17, Ang1 fl/fl$^{Nestin:Cre}$ n = 15, from 4 independent litters). Unpaired two-sided T-Test, ***p=0.0001. **e**, Images of Ang1 fl/fl (control) vs Ang1 fl/fl$^{Nestin:Cre}$ (CNS-Ang1 deleted) embryos from E11.5 to E13.5. Scale bar 1 mm. **f**, Transverse thick sections of Ang1 fl/fl and Ang1 fl/fl$^{Nestin:Cre}$ immunostained for Nestin to visualize neural progenitor projections. Scale bar 100μm. **g**,**h**, Analysis at brachial (**g**) and thoracic (**h**) levels of SC tissue total area. Graphs show mean±SEM (Ang1 fl/fl n=9, Ang1 fl/fl$^{Nestin:Cre}$ n=10). Unpaired two-sided T-Test. **i**, Images of transverse sections at thoracic level of Ang1 fl/fl and Ang1 fl/fl$^{Nestin:Cre}$ E12.5 embryos showing the pMN domain immunostained for Olig2 and Sox10. Bracket: pMN; Open arrowheads indicate OPCs in the pMN and filled arrowheads OPCs in the MZ. Scale bar 50 μm. **j**, Quantification of OPCs in the VZ and MZ of Ang1 fl/fl and Ang1 fl/fl$^{Nestin:Cre}$, normalized to controls (Ang1fl/fl). **k**, Analysis of the number of $Olig2^+$ progenitors in the pMN. **l**, Ratio of pMN $Sox10^+$ cells within the total number of $Olig2^+$ pMN progenitor cells. For j-l: Graphs show mean±SEM (Ang1 fl/fl n=7, Ang1 fl/fl$^{Nestin:Cre}$ n=8, of 3 independent litters). Unpaired two-sided T-test. j: VZ ***p=0.0006; MZ **p=0.0028; l: Sox10% * p=0.0180. **m**, *ISH* for *Pdgfra* in 18 μm transverse sections of E12.5 Ang1 fl/fl and Ang1 fl/fl$^{Nestin:Cre}$ embryo at brachial and thoracic levels. Data is representative from Ang1 fl/fl n=7, Ang1 fl/fl$^{Nestin:Cre}$ n=8, from 3 independent litters. Arrowheads indicate *Pdgfra+* cells. Scale bar 100μm. **n**, Transverse sections at brachial level of Ang1 fl/fl and Ang1 fl/fl$^{Nestin:Cre}$ E16.5 embryos immunostained for Olig2. Scale bar 100μm. **o**, Quantification of $Olig2^+$ OL lineage cells in E16.5 Ang1 fl/fl and Ang1 fl/fl$^{Nestin:Cre}$ embryos, normalized to control (Ang1 fl/fl) littermates. Graphs show mean±SEM (Ang1 fl/fl n=10, Ang1 fl/fl$^{Nestin:Cre}$ n=13, of 3 independent litters). Unpaired two-sided T-test.

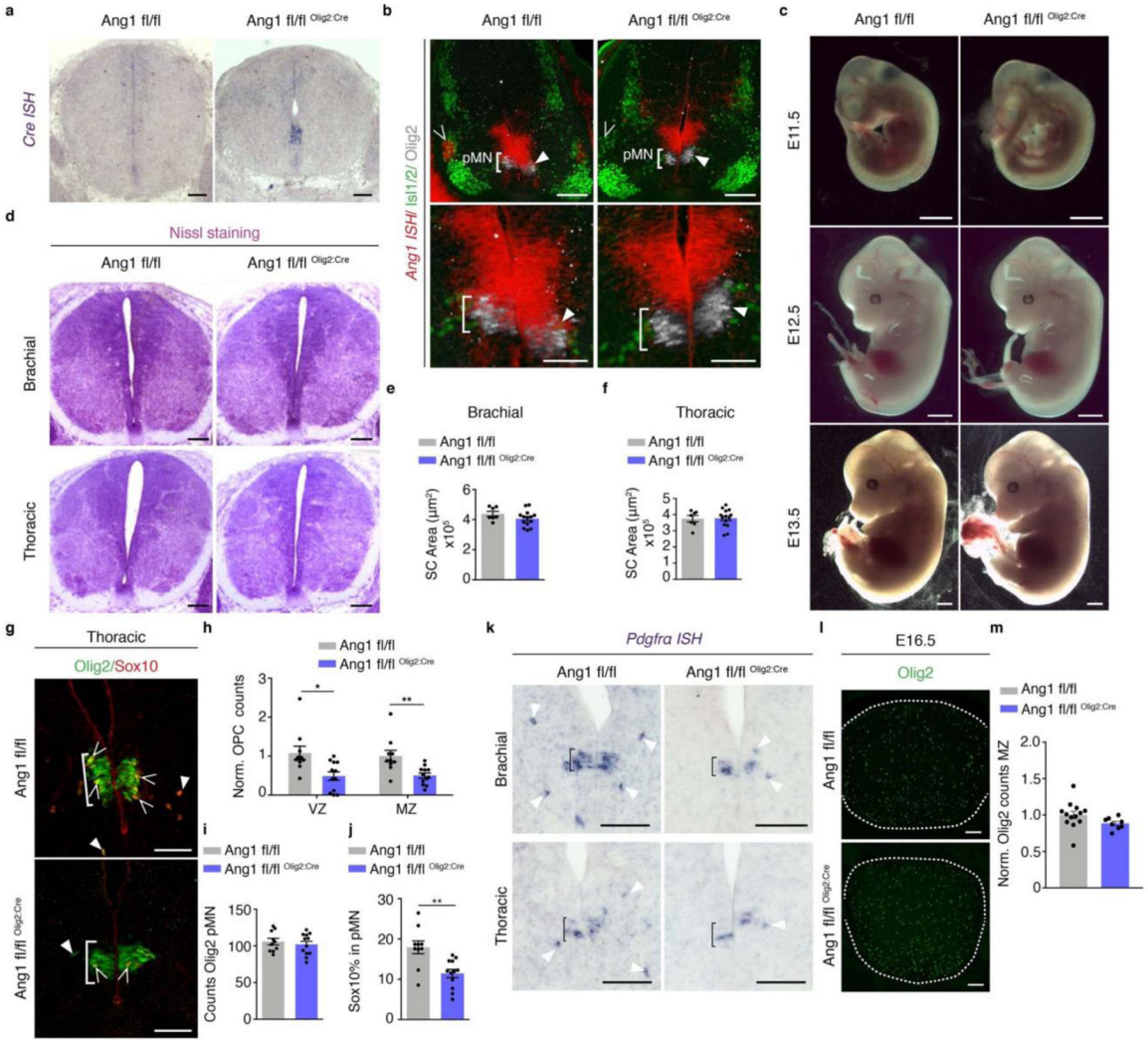

Extended Data Fig. 4 |. Ang1 fl/fl$^{Olig2:Cre}$ embryos and SC gross morphology appear normal, but show OPC specification defects.

a, *ISH* for *Cre recombinase* in transverse sections of E12.5 Ang1 fl/fl and Ang1 fl/fl$^{Olig2:Cre}$ embryo showing *Cre* expression only in the pMN domain. Data is representative from at least 3 independent embryos per genotype, from 2 litters. Scale bar 100µm. **b**, *ISH* for *Ang1* (pseudo-coloured in red) combined with immunostaining for Olig2 and Isl1/2. Filled arrowheads point to the pMN and open arrowheads point to MNs in transverse sections of E11.5 Ang1 fl/fl and Ang1 fl/fl$^{Olig2:Cre}$ embryos. Note the efficient deletion of *Ang1* in the pMN and MNs of Ang1 fl/fl$^{Olig2:Cre}$ embryos. Data is representative from at least 3 independent embryos per genotype, from 2 litters. Scale bar 50µm (inset) 100µm (upper panel). **c**, Images of Ang1 fl/fl (control) vs Ang1 fl/fl$^{Olig2:Cre}$ embryos from E11.5 to E13.5. Scale bar 1 mm. **d**, Nissl staining in transverse sections of Ang1 fl/fl and Ang1 fl/fl$^{Olig2:Cre}$ E12.5 embryos. Data is representative from at least 3 embryos per genotype, from 2 independent litters. Scale bar 100µm. **e**,**f**, Analysis at brachial (**e**) and thoracic (**f**) levels of SC total area. Graphs show mean±SEM (Ang1 fl/fl n=7, Ang1 fl/fl$^{Olig2:Cre}$ n=14, from 3 independent litters). Unpaired two-sided T-Test. **g**, Images of transverse sections at thoracic

level of Ang1 fl/fl (control) and Ang1 fl/fl$^{Olig2:Cre}$ E12.5 embryos immunostained for Olig2 and Sox10. Bracket: pMN; Filled arrowhead point to MZ OPCs and open arrowheads to VZ OPCs. Scale bar 50μm. **h**, Quantification of OPCs in the VZ and MZ of Ang1 fl/fl and Ang1 fl/fl$^{Olig2:Cre}$, normalized to controls (Ang1fl/fl). **i**, Analysis of the number of Olig2^{+} progenitors in the pMN. **j**, Ratio of pMN Sox10^{+} cells within the total number of Olig2^{+} pMN progenitor cells. For **h-j**: Graphs show mean±SEM (Ang1 fl/fl n=10, Ang1 fl/fl$^{Olig2:Cre}$ n=12, of 3 independent litters). Unpaired two-sided T-test. h: VZ *p=0.0110; MZ **p=0.0076; j: Sox10% **p=0.0033. **k**, *ISH* for *Pdgfra* in 40 μm transverse sections of E12.5 Ang1 fl/fl and Ang1 fl/fl$^{Olig2:Cre}$ embryo at brachial and thoracic levels. Data is representative from Ang1 fl/fl n=7 and Ang1 fl/fl$^{Olig2:Cre}$ n=9, from 2 independent litters. Arrowheads indicate *Pdgfra* positive cells. Scale bar 100μm. **l**, Transverse sections at brachial level of Ang1 fl/fl (control) and Ang1 fl/fl$^{Olig2:Cre}$ E16.5 embryos immunostained for Olig2. Scale bar 100μm. **m**, Quantification of Olig2^{+} cells (OL lineage) in E16.5 Ang1 fl/fl and Ang1 fl/fl$^{Olig2:Cre}$ embryos, normalized to control (Ang1 fl/fl) littermates. Graphs show mean±SEM (Ang1 fl/fl n=13, Ang1 fl/fl$^{Olig2:Cre}$ n=8, of 3 independent litters). Unpaired two-sided T-test.

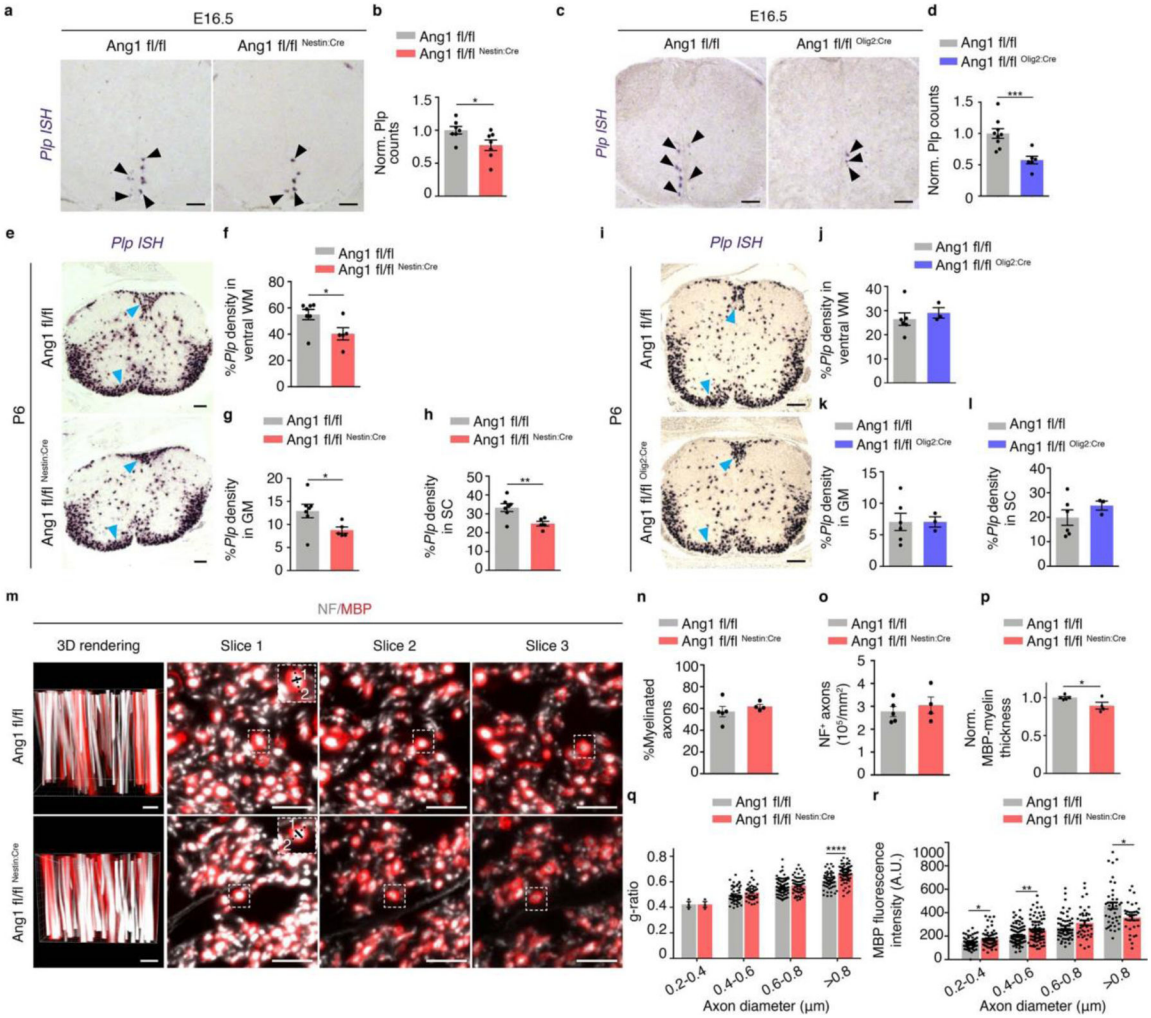

Extended Data Fig. 5 |. Impaired OL differentiation and maturation in neural specific Ang1-deficient mice.

a, Transverse sections at brachial level of Ang1 fl/fl (control) and Ang1 fl/fl$^{Nestin:Cre}$ E16.5 embryos hybridized with an *ISH* probe for *Plp*. Arrowheads point to *Plp*$^{+}$ pre-OLs lining the ventral funiculus. Scale bar 100μm. **b**, Quantification of *Plp*$^{+}$ cell counts in E16.5 Ang1 fl/fl and Ang1 fl/fl$^{Nestin:Cre}$ embryos, normalized to control (Ang fl/fl) littermates. Graph show mean±SEM (Ang1 fl/fl n=7, Ang1 fl/fl$^{Nestin:Cre}$ n=7, of 3 independent litters). Unpaired two-sided T-test, *p=0.0413. **c**, Transverse sections at brachial level of Ang1 fl/fl (control) and Ang1 fl/fl$^{Olig2:Cre}$ E16.5 embryos hybridized with an *ISH* probe for *Plp*. Arrowheads point to *Plp*$^{+}$ pre-OLs lining the ventral funiculus. Scale bar 100μm. **d**, Quantification of *Plp*$^{+}$ cell counts in E16.5 Ang1 fl/fl and Ang1 fl/fl$^{Olig2:Cre}$ embryos, normalized to control (Ang fl/fl) littermates. Graph show mean±SEM (Ang1 fl/fl n=9, Ang1 fl/fl$^{Olig2:Cre}$ n=6, of 2 independent litters). Unpaired two-sided T-test, ***p=0.0008. **e**, Transverse sections from Ang1 fl/fl and Ang1 fl/fl$^{Nestin:Cre}$ neonatal SC at postnatal day (P6) hybridized with an *ISH* probe for *Plp*. Blue arrowheads indicate white matter (WM). The rest of the SC is grey matter (GM). Scale bar 100μm. **f-h**, *Plp*$^{+}$ density (percentage of the surface occupied by *Plp* signal) was measured in Ang1 fl/fl and Ang1 fl/fl$^{Nestin:Cre}$ in ventral white matter (WM) and shown as %*Plp* of ventral WM area (**f**). *Plp*$^{+}$ density was also measured in the developing grey matter (GM) (**g**), and shown as %*Plp* of GM area, and in the entire SC shown as %*Plp* of total SC area (**h**). Graphs show mean±SEM (Ang1 fl/fl n=7, Ang1 fl/fl$^{Olig2:Cre}$ n=5, of 2 independent litters). Unpaired two-sided T-test (WM *p=0.0359; GM *p=0.0333; SC **p=0.0064). **i**, Transverse sections from Ang1 fl/fl and Ang1 fl/fl$^{Olig2:Cre}$ neonatal SC at postnatal day (P6) hybridized with an *ISH* probe for *Plp*. Blue arrowheads indicate white matter (WM). The rest of the SC is grey matter (GM). Scale bars 100μm. **j–l**, *Plp*$^{+}$ density was measured in Ang1 fl/fl and Ang1 fl/fl$^{Olig2:Cre}$ in ventral white matter (WM) and shown as %*Plp* of ventral WM area (**j**). *Plp*$^{+}$ density was also measured in the developing grey matter (GM) (**k**), and shown as %*Plp* of GM area, and in the entire SC (**l**), and shown as %*Plp* of total SC area. Graphs show mean±SEM (Ang1 fl/fl n=6, Ang1 fl/fl$^{Olig2:Cre}$ n=3, of 2 independent litters). Unpaired two-sided T-Test. **m**, 3D reconstruction (left panels) and serial slices spaced by approx. 5 μm distance (right panels) of ventral funiculus field of view showing MBP-myelinated NF^{+} axons of Ang1 fl/fl (upper panels) and Ang1 fl/fl$^{Nestin:Cre}$ (lower panels). Insets in dashed boxes in the right upper corner are shown for Slice 1 of both genotypes indicating an example of diameter measurements for NF^{+} axons (1-continuous line) and fibers NF^{+} axons + MBP^{+}-myelin ring (2- dashed line). Dashed boxes in middle of the Slice 2 and 3 follow the same axon at increasing depths from Slice 1. Scale bar (left-3D reconstruction): 3 μm and right panels: 5 μm. **n**,**o**, Percentage of myelinated axons in a slice of field of view (**n**) and quantification of the total number of axons (**o**) in the ventral funiculus of Ang1 fl/fl and Ang1 fl/fl$^{Nestin:Cre}$ p6 SCs. Graphs show mean±SEM (Ang1 fl/fl n=5, Ang1 fl/fl$^{Nestin:Cre}$ n=4 pups, of 2 independent litters). Unpaired two-sided T-test. **p**, Analysis of MBP-based myelin thickness of NF^{+} axons from the ventral funiculus of Ang1 fl/fl and Ang1 fl/fl$^{Nestin:Cre}$ p6 SCs. Values were normalized to control (Ang1fl/fl) littermates. Graphs show mean±SEM (values for four images were averaged for total of Ang1 fl/fl n=5, Ang1 fl/fl $^{Nestin:Cre}$ n=4 pups, from 2 independent litters). Unpaired two-sided T-test, *p=0.0390. **q**, g-ratio measured in MBP-surrounded NF^{+} axons from the ventral funiculus classified in four bins of axon calibre of Ang1 fl/fl and

Ang1 fl/fl$^{Nestin:Cre}$ P6 SCs. Graphs show mean±SEM (Bin 0.2–0.4: Ang1 fl/fl n=3, Ang1 fl/fl$^{Nestin:Cre}$ n=3 axons; Bin 0.4–0.6: Ang1 fl/fl n=53, Ang1 fl/fl$^{Nestin:Cre}$ n=44 axons; Bin 0.6–0.8: Ang1 fl/fl n=88, Ang1 fl/fl $^{Nestin:Cre}$ n=61 axons; Bin >0.8: Ang1 fl/fl n=58, Ang1 fl/fl $^{Nestin:Cre}$ n=63 axons). In total, Ang1 fl/fl =5 [total 191 axons], Ang1 fl/fl $^{Nestin:Cre}$ =4 [total:171 axons] pups, of 2 independent litters were analysed. Mann-Whitney two-sided U-test, ****p<0.0001. **r**, Analysis of MBP fluorescence intensity surrounding NF^{+} axons of a ventral funiculus field of view of Ang1 fl/fl and Ang1 fl/fl$^{Nestin:Cre}$ P6 SCs. Graphs show mean±SEM (Bin 0.2–0.4: Ang1 fl/fl n=58, Ang1 fl/fl $^{Nestin:Cre}$ n=60 axons; Bin 0.4–0.6: Ang1 fl/fl n=92, Ang1 fl/fl$^{Nestin:Cre}$ n=82 axons; Bin 0.6–0.8: Ang1 fl/fl n=55 Ang1 fl/fl $^{Nestin:Cre}$ n=39 axons; Bin >0.8: Ang1 fl/fl n=41, Ang1 fl/fl$^{Nestin:Cre}$ n=31 axons). In total Ang1 fl/fl =5 [246 total axons] and Ang1 fl/fl$^{Nestin:Cre}$ =4 [total 212 axons] pups, of 2 independent litters were analysed. Mann-Whitney two-sided U-test, Bin 0.2–0.4 *p=0.0367, Bin 0.4–0.6 **p=0.0021, Bin>0.8 *p=0.0319.

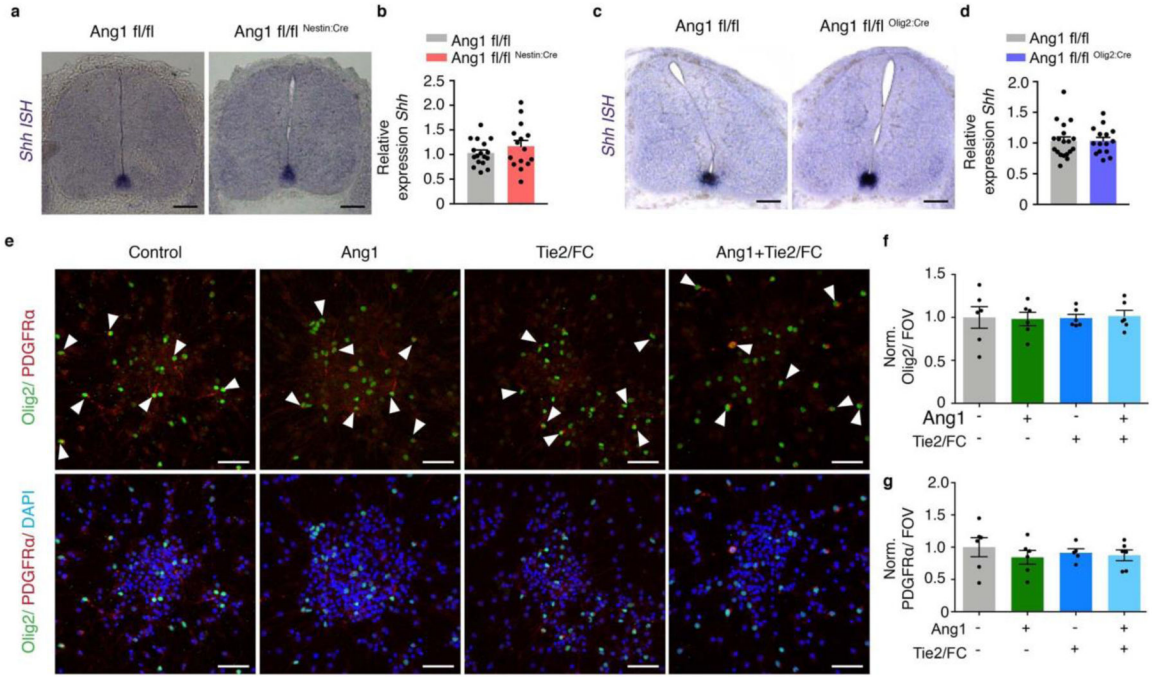

Extended Data Fig. 6 |. NPC-derived Ang1 promotes OPC specification via a paracrine mechanism.

a,**b**, *ISH* for *Shh* in transverse sections of embryo SCs (**a**) and relative expression of *Shh* mRNA (**b**) in the neural compartment of E12.5 Ang1 fl/fl vs Ang1 fl/fl$^{Nestin:Cre}$ embryos. Graphs show mean±SEM (Ang1 fl/fl n=17, Ang1 fl/fl$^{Nestin:Cre}$ n=15, of 4 independent litters). Unpaired two-sided T-test. Scale bar 100μm (**a**). **c**,**d**, *ISH* for *Shh* in transverse sections of embryo SCs (c) and relative expression of *Shh* mRNA (**d**) in the neural compartment of E12.5 Ang1 fl/fl v/s Ang1 fl/fl$^{Olig2:Cre}$. Graphs show mean±SEM (Ang1 fl/fl n=19, Ang1 fl/fl$^{Olig2:Cre}$ n=15, of 4 independent litters). Unpaired two-sided T-test. Scale bar 100μm (**c**). **e**, Representative images of neural-progenitors derived NSPs derived from E11.5 wild-type embryo SCs and cultured for 72 h in differentiation conditions and treated with vehicle (control), Ang1 (100 mg/mL) and/or Tie2/FC (2 μg/mL). *In vitro*

cultures were immunostained for Olig2 (labelling neural progenitors and OL lineage cells) and PDFGRα (labelling committed OPCs, arrowheads). Scale bar 50μm. **f**, Quantification of Olig2^{+} cells per field of view (FOV) of NSP *in vitro* cultures treated as in (**e**), normalized to control conditions. **g**, Quantification of PDGFRα^{+} cells per field of view (FOV) of NSP *in vitro* cultures treated as in (**e**), normalized to control conditions. Graphs show mean±SEM (n= 6 (independent experiments) isolated and differentiated NSPs cell cultures), one-way ANOVA.

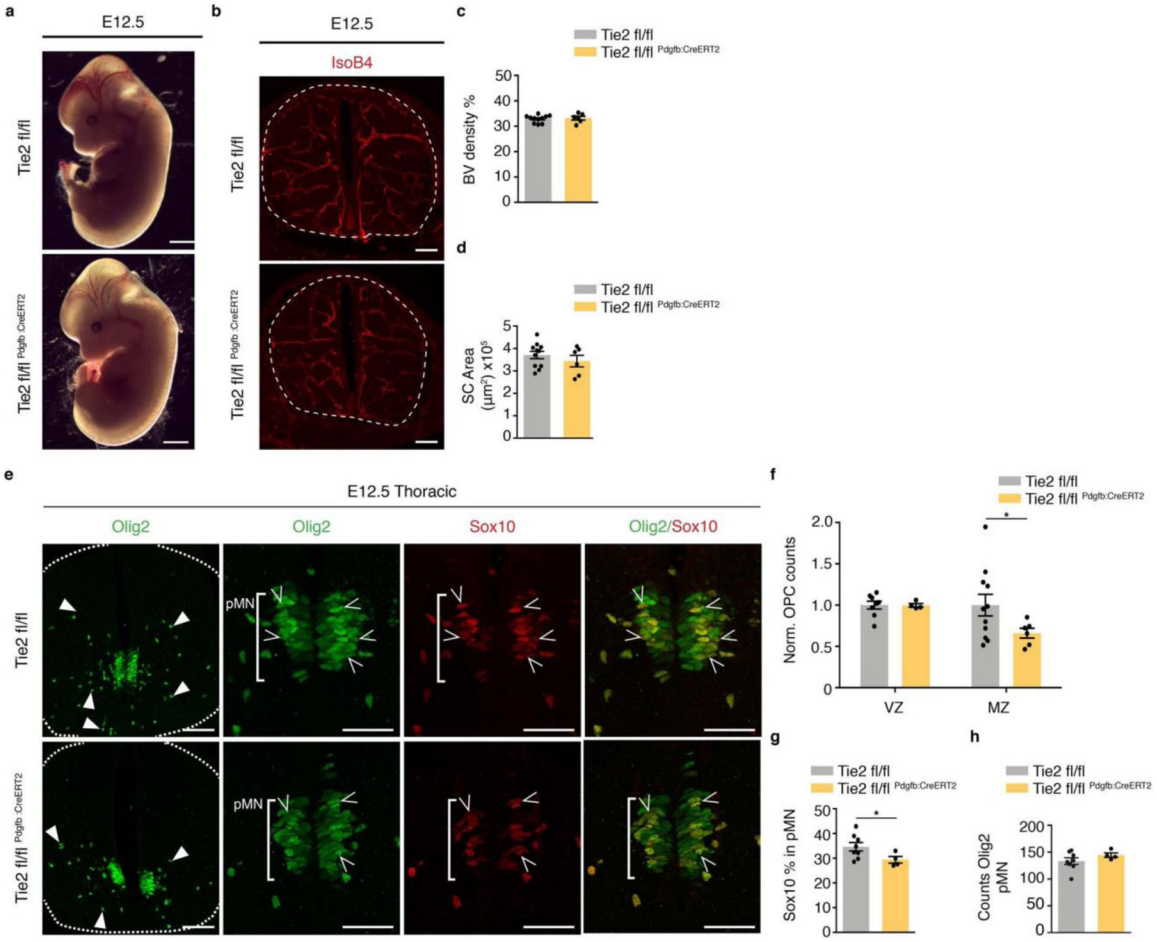

Extended Data Fig. 7 |. Tie2 fl/fl$^{Pdgfb:CreERT2}$ embryos and SC gross morphology appear normal, but show OPC specification defects.

a, Images of E12.5 Tie2 fl/fl (control) and Tie2 fl/fl$^{Pdgfb:CreERT2}$ embryos. Scale bar 1 mm. **b**, Tie2 fl/fl and Tie2 fl/fl$^{Pdgfb:CreERT2}$ E12.5 transverse 40 μm sections stained with IsoB4 showing the SC. Scale bar 100μm. **c**, Blood vessel (BV) density quantification of Tie2 fl/fl (control) and Tie2 fl/fl$^{Pdgfb:CreERT2}$ and normalized to control (Tie2 fl/fl) littermates (**c**). **d**, Analysis of SC total area in Tie2 fl/fl and Tie2 fl/fl$^{Pdgfb:CreERT2}$ E12.5 embryos (**d**). For **c**,**d**: Graphs show mean±SEM (Tie2 fl/fl n=11, Tie2 fl/fl$^{Pdgfb:CreERT2}$ n= 6, of 2 independent litters). Unpaired two-sided T-test. **e**, Images of thoracic transverse sections of Tie2 fl/fl and Tie2 fl/fl$^{Pdgfb:CreERT2}$ E12.5 SCs. Left images: entire SC immunostained with Olig2. Right images: pMN domain immunostained for Olig2 and Sox10. Bracket: pMN; open arrowheads

indicate OPCs in the pMN and filled arrowheads in the MZ. Scale bars 100μm (left panels) and 50 μm (right (pMN) panels). **f**, Quantification of OPCs in the VZ (Tie2 fl/fl n=8, Tie2 fl/fl$^{Pdgfb:Cre}$ n=4, of 2 independent litters) and MZ (Tie2 fl/fl n=11, Tie2 fl/fl$^{Pdgfb:Cre}$ n=6, of 2 independent litters) of Tie2 fl/fl and Tie2 fl/fl$^{Pdgfb:CreERT2}$, normalized to controls (Tie2 fl/fl). Graphs show mean±SEM. Unpaired two-sided T-test (MZ *p=0.0338). **g**, Percentage of pMN Sox10^{+} cells within the total number of Olig2^{+} pMN progenitor cells. **h**, Analysis of Olig2^{+} progenitor number in the pMN. Graphs show mean±SEM. Unpaired two-sided T-test (Sox10% *p=0.0379). Graphs (**g**) and (**h**) show mean±SEM (Tie2 fl/fl n=8, Tie2 fl/fl$^{Pdgfb:Cre}$ n= 4, of 2 independent litters). Unpaired two-sided T-test.

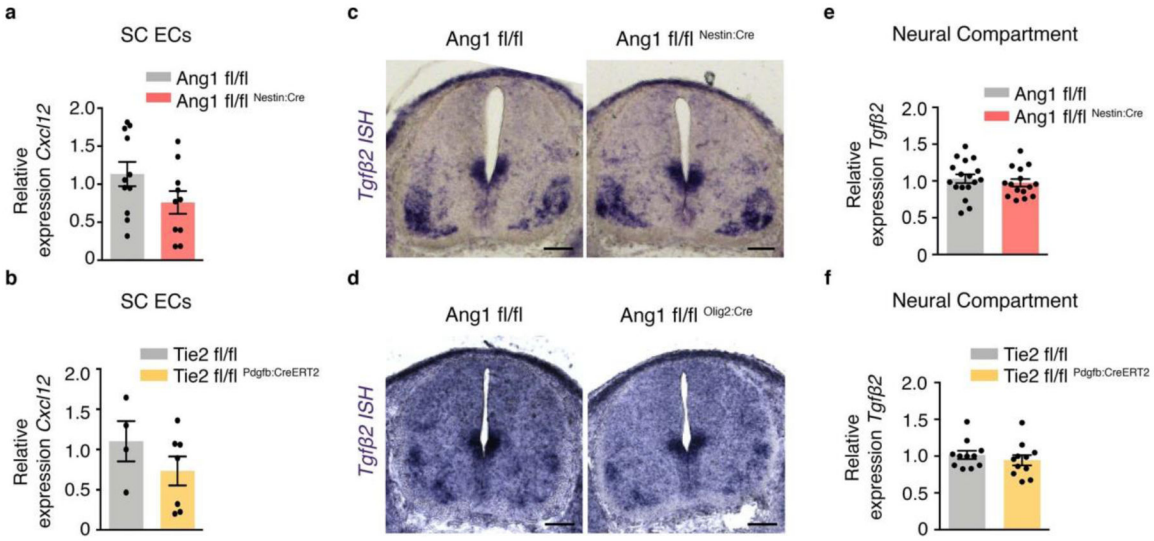

Extended Data Fig. 8 |. *Cxcl12* and *Tgfβ2* are unchanged in Ang1 fl/fl$^{Nestin:Cre}$ Tie2 fl/fl$^{Pdgfb:CreERT2}$ embryo SCs.

a, Relative expression of *Cxcl12* mRNA in CD31^{+}ECs sorted from Ang1 fl/fl and Ang1 fl/fl$^{Nestin:Cre}$ E12.5 SCs. Graphs show mean±SEM (Ang1 fl/fl n=11, Ang1 fl/fl$^{Nestin:Cre}$ n=10, of 3 independent litters). Unpaired two-sided T-test. **b**, Relative expression of *Cxcl12* mRNA in CD31^{+}ECs sorted from Tie2 fl/fl and Tie2 fl/fl$^{Pdgfb:CreERT2}$ SCs. Graphs show mean±SEM (Tie2 fl/fl n=4, Tie2 fl/fl$^{Pdgfb:CreERT2}$ n=7, of 2 independent litters). Unpaired two-sided T-test. **c**,**d**, *ISH* for *Tgfβ2* in transverse sections from E12.5 Ang1 fl/fl vs Ang1 fl/fl$^{Nestin:Cre}$ (**c**) and Ang1 fl/fl vs Ang1 fl/fl$^{Olig2:Cre}$ (**d**) embryos. Scale bar 100μm. **e**, Relative expression of *Tgfβ2* mRNA from CD31^{-} negative selection (isolated neural compartment) from Ang1 fl/fl and Ang1 fl/fl$^{Nestin:Cre}$ E12.5 SCs. Graphs show mean±SEM (Ang1 fl/fl n=17, Ang1 fl/fl$^{Nestin:Cre}$ n=15, from 4 independent litters). Unpaired two-sided T-test. **f**, Relative expression of *Tgfβ2* mRNA from CD31^{-} negative selection (isolated neural compartment) from Tie2 fl/fl and Tie2 fl/fl$^{Pdgfb:CreERT2}$ E12.5 SCs. Graphs show mean±SEM (Tie2 fl/fl n=11, Tie2 fl/fl $^{Pdgfb:CreERT2}$ n=11, from 3 independent litters). Unpaired two-sided T-test.

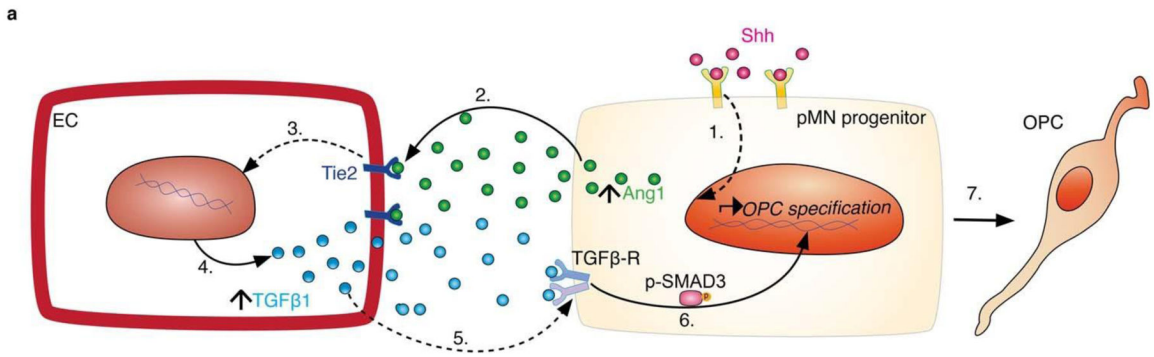

Extended Data Fig. 9 |. Model of bi-directional NPC-EC communication regulating OPC specification.

a, Step-by-step model of the identified NPC-EC bidirectional crosstalk required for OPC specification. ***1 and 2***. Floor plate/Notochord-derived Shh transcriptionally regulates *Ang1* expression in NPCs. ***3***. NPC-derived Ang1 produced binds and activates Tie2 in ECs. ***4 and 5***. Tie2 activation triggers *Tgfβ1* transcriptional upregulation in ECs. ***6***. TGFβ1, signals back to pMN NPCs inducing phosphorylation of its intracellular effector SMAD3. ***7***. NPCs are induced to specify their fate to OPCs.

Supplementary Material

Refer to Web version on PubMed Central for supplementary material.

Acknowledgements

We thank K. Armin-Nave and W. Möbius (Max Planck Institute of Experimental Medicine, Göttingen) for their expert advice during the study. We thank S. Quaggin (Northwestern University) for providing the Ang1 fl/fl mice; T.M. Jessell and T. Marquardt (University of Göttingen) for the Olig2:Cre mice; H. Monyer (DKFZ) for the Nestin:Cre mice; M. Fruttiger (University College London) for providing the Pdgfb:CreERT2 mice; and M. Hecker (Heidelberg University) for providing the Tie2Cre:ERT2 mice. We thank P. Carmeliet (VIB, KULeuven) and H. Marti (Heidelberg University) for providing the *Shh* and the *Ang1* and *Tie2* ISH probes, respectively. We also thank the Nikon Imaging Center at Heidelberg University for providing their imaging facility. We thank P. Himmels for her help with the mTmGNestin:Cre mice and the entire Ruiz de Almodovar's group for helpful discussions. This work was supported by ERC-CoG (864875); by a grant of the Deutsche Forschungsgemeinschaft (DFG) from FOR2325 ('Interactions at the neurovascular interface' (to C.R.d.A.)); DFG grants from SFB1366 ('Vascular control of organ function', project number 39404578 (to H.G.A. and C.R.d.A.)); DFG grant of the SFB873 ('Maintenance and differentiation of stem cells in health and disease' (to C.R.d.A.)), DFG grant of the SFB1158 ('From nociception to chronic pain: structure–function properties of neural pathways and their reorganization' (to C.R.d.A.)), by funds from the Baden-Württemberg Stiftung special programme 'Angioformatics single cell platform' (to C.R.d.A and H.G.A), by the European Research Council 787181 'Angiomature' (to H.G.A.), by the Hertie Foundation (medMS MyLab program, P1180016 (to L.S.)), by the National Multiple Sclerosis Society (FG-1902-33617 (to L.S.)) and by the National Institutes of Health (P30 DK114857 (PI-SEQ)). I.P. was supported by a PhD fellowship, Becas Chile (CONICYT).

References

1. Fancy SP, Chan JR, Baranzini SE, Franklin RJ & Rowitch DH Myelin regeneration: a recapitulation of development? Annu Rev. Neurosci 34, 21–43 (2011). [PubMed: 21692657]
2. Rowitch DH & Kriegstein AR Developmental genetics of vertebrate glial-cell specification. Nature 468, 214–222 (2010). [PubMed: 21068830]
3. Bergles DE & Richardson WD Oligodendrocyte development and plasticity. Cold Spring Harb. Perspect. Biol 8, a020453 (2015). [PubMed: 26492571]

4. Yu K, McGlynn S & Matise MP Floor plate-derived Sonic hedgehog regulates glial and ependymal cell fates in the developing spinal cord. Development 140, 1594–1604 (2013). [PubMed: 23482494]
5. Farreny MAet al.FGF signaling controls Shh-dependent oligodendroglial fate specification in the ventral spinal cord. Neural Dev. 13, 3 (2018). [PubMed: 29519242]
6. Dias JM, Alekseenko Z, Applequist JM & Ericson J Tgfβ signaling regulates temporal neurogenesis and potency of neural stem cells in the CNS. Neuron 84, 927–939 (2014). [PubMed: 25467979]
7. Dutta DJet al.Combinatorial actions of Tgfβ and Activin ligands promote oligodendrocyte development and CNS myelination. Development141, 2414–2428 (2014). [PubMed: 24917498]
8. Rabadan MAet al.Jagged2 controls the generation of motor neuron and oligodendrocyte progenitors in the ventral spinal cord. Cell Death Differ. 19, 209–219 (2012). [PubMed: 21720386]
9. Cui XYet al.NB-3/Notch1 pathway via Deltex1 promotes neural progenitor cell differentiation into oligodendrocytes. J. Biol. Chem279, 25858–25865 (2004). [PubMed: 15082708]
10. Paredes I, Himmels P & Ruiz de Almodovar C Neurovascular communication during CNS development. Dev. Cell 45, 10–32 (2018). [PubMed: 29634931]
11. Himmels Pet al.Motor neurons control blood vessel patterning in the developing spinal cord. Nat. Commun8, 14583 (2017). [PubMed: 28262664]
12. Augustin HG & Koh GY Organotypic vasculature: from descriptive heterogeneity to functional pathophysiology. Science 357, eeal2379 (2017).
13. Rafii S, Butler JM & Ding BS Angiocrine functions of organ-specific endothelial cells. Nature 529, 316–325 (2016). [PubMed: 26791722]
14. Ramasamy SK, Kusumbe AP & Adams RH Regulation of tissue morphogenesis by endothelial cell-derived signals. Trends Cell Biol. 25, 148–157 (2015). [PubMed: 25529933]
15. Lorenz Let al.Mechanosensing by β1 integrin induces angiocrine signals for liver growth and survival. Nature562, 128–132 (2018). [PubMed: 30258227]
16. Hu Jet al.Endothelial cell-derived angiopoietin-2 controls liver regeneration as a spatiotemporal rheostat. Science343, 416–419 (2014). [PubMed: 24458641]
17. Augustin HG, Koh GY, Thurston G & Alitalo K Control of vascular morphogenesis and homeostasis through the angiopoietin–Tie system. Nat. Rev. Mol. Cell Biol 10, 165–177 (2009). [PubMed: 19234476]
18. Delile Jet al.Single cell transcriptomics reveals spatial and temporal dynamics of gene expression in the developing mouse spinal cord. Development146, dev173807 (2019). [PubMed: 30846445]
19. Tekki-Kessaris Net al.Hedgehog-dependent oligodendrocyte lineage specification in the telencephalon. Development128, 2545–2554 (2001). [PubMed: 11493571]
20. Li Yet al.Sonic hedgehog (Shh) regulates the expression of angiogenic growth factors in oxygen-glucose-deprived astrocytes by mediating the nuclear receptor NR2F2. Mol. Neurobiol47, 967–975 (2013). [PubMed: 23378030]
21. Pola Ret al.The morphogen Sonic hedgehog is an indirect angiogenic agent upregulating two families of angiogenic growth factors. Nat. Med7, 706–711 (2001). [PubMed: 11385508]
22. Yam PT, Langlois SD, Morin S & Charron F Sonic hedgehog guides axons through a noncanonical, Src-family-kinase-dependent signaling pathway. Neuron 62, 349–362 (2009). [PubMed: 19447091]
23. Langlois SD, Morin S, Yam PT & Charron F Dissection and culture of commissural neurons from embryonic spinal cord. J. Vis. Exp 39, 1773 (2010).
24. Agius Eet al.Converse control of oligodendrocyte and astrocyte lineage development by Sonic hedgehog in the chick spinal cord. Dev. Biol270, 308–321 (2004). [PubMed: 15183716]
25. Touahri Yet al.Sulfatase 1 promotes the motor neuron-to-oligodendrocyte fate switch by activating Shh signaling in Olig2 progenitors of the embryonic ventral spinal cord. J. Neurosci32, 18018–18034 (2012). [PubMed: 23238718]
26. Sato TNet al.Distinct roles of the receptor tyrosine kinases Tie-1 and Tie-2 in blood vessel formation. Nature376, 70–74 (1995). [PubMed: 7596437]
27. Jeansson Met al.Angiopoietin-1 is essential in mouse vasculature during development and in response to injury. J. Clin. Invest121, 2278–2289 (2011). [PubMed: 21606590]

28. Kim KH, Nakaoka Y, Augustin HG & Koh GY Myocardial angiopoietin-1 controls atrial chamber morphogenesis by spatiotemporal degradation of cardiac jelly. Cell Rep. 23, 2455–2466 (2018). [PubMed: 29791855]
29. Tronche Fet al.Disruption of the glucocorticoid receptor gene in the nervous system results in reduced anxiety. Nat. Genet23, 99–103 (1999). [PubMed: 10471508]
30. Pringle NP & Richardson WD A singularity of PDGF alpha-receptor expression in the dorsoventral axis of the neural tube may define the origin of the oligodendrocyte lineage. Development 117, 525–533 (1993). [PubMed: 8330523]
31. Dessaud Eet al.Interpretation of the Sonic hedgehog morphogen gradient by a temporal adaptation mechanism. Nature450, 717–720 (2007). [PubMed: 18046410]
32. Simons M & Nave KA Oligodendrocytes: myelination and axonal support. Cold Spring Harb. Perspect. Biol 8, a020479 (2015). [PubMed: 26101081]
33. Motoike Tet al.Universal GFP reporter for the study of vascular development. Genesis28, 75–81 (2000). [PubMed: 11064424]
34. Savant Set al.The orphan receptor Tie1 controls angiogenesis and vascular remodeling by differentially regulating Tie2 in Tip and stalk cells. Cell Rep. 12, 1761–1773 (2015). [PubMed: 26344773]
35. Chu Met al.Angiopoietin receptor Tie2 is required for vein specification and maintenance via regulating COUP-TFII. eLife5, e21032 (2016). [PubMed: 28005008]
36. Tsai HHet al.Oligodendrocyte precursors migrate along vasculature in the developing nervous system. Science351, 379–384 (2016). [PubMed: 26798014]
37. Palazuelos J, Klingener M & Aguirre A TGFβ signaling regulates the timing of CNS myelination by modulating oligodendrocyte progenitor cell cycle exit through SMAD3/4/FoxO1/Sp1. J. Neurosci 34, 7917–7930 (2014). [PubMed: 24899714]
38. Mecha Met al.Expression of TGF-βs in the embryonic nervous system: analysis of interbalance between isoforms. Dev. Dyn237, 1709–1717 (2008). [PubMed: 18498095]
39. Massague JTGFβ signalling in context. Nat. Rev. Mol. Cell Biol13, 616–630 (2012). [PubMed: 22992590]
40. Marklund Uet al.Domain-specific control of neurogenesis achieved through patterned regulation of Notch ligand expression. Development137, 437–445 (2010). [PubMed: 20081190]
41. Barber Met al.Vascular-derived vegfa promotes cortical interneuron migration and proximity to the vasculature in the developing forebrain. Cereb. Cortex28, 2577–2593 (2018). [PubMed: 29901792]
42. Segarra M, Aburto MR, Hefendehl J & Acker-Palmer A Neurovascular interactions in the nervous system. Annu. Rev. Cell Dev. Biol 35, 615–635 (2019). [PubMed: 31590587]
43. Arita Yet al.Myocardium-derived angiopoietin-1 is essential for coronary vein formation in the developing heart. Nat. Commun5, 4552 (2014). [PubMed: 25072663]
44. Kessaris Net al.Competing waves of oligodendrocytes in the forebrain and postnatal elimination of an embryonic lineage. Nat. Neurosci9, 173–179 (2006). [PubMed: 16388308]
45. Yuen TJet al.Oligodendrocyte-encoded HIF function couples postnatal myelination and white matter angiogenesis. Cell158, 383–396 (2014). [PubMed: 25018103]
46. Muzumdar MD, Tasic B, Miyamichi K, Li L & Luo L A global double-fluorescent Cre reporter mouse. Genesis 45, 593–605 (2007). [PubMed: 17868096]
47. Claxton Set al.Efficient, inducible Cre-recombinase activation in vascular endothelium. Genesis46, 74–80 (2008). [PubMed: 18257043]
48. Liu HThe role of EphB/ephrinB in inflammation. PhD thesis, Universität Heidelberghttps://archiv.ub.uni-heidelberg.de/volltextserver/15772/1/Hui%20Liu%20thesis%202611%20final.pdf (2013).
49. Hua ZL, Smallwood PM & Nathans J Frizzled3 controls axonal development in distinct populations of cranial and spinal motor neurons. eLife 2, e01482 (2013) [PubMed: 24347548]

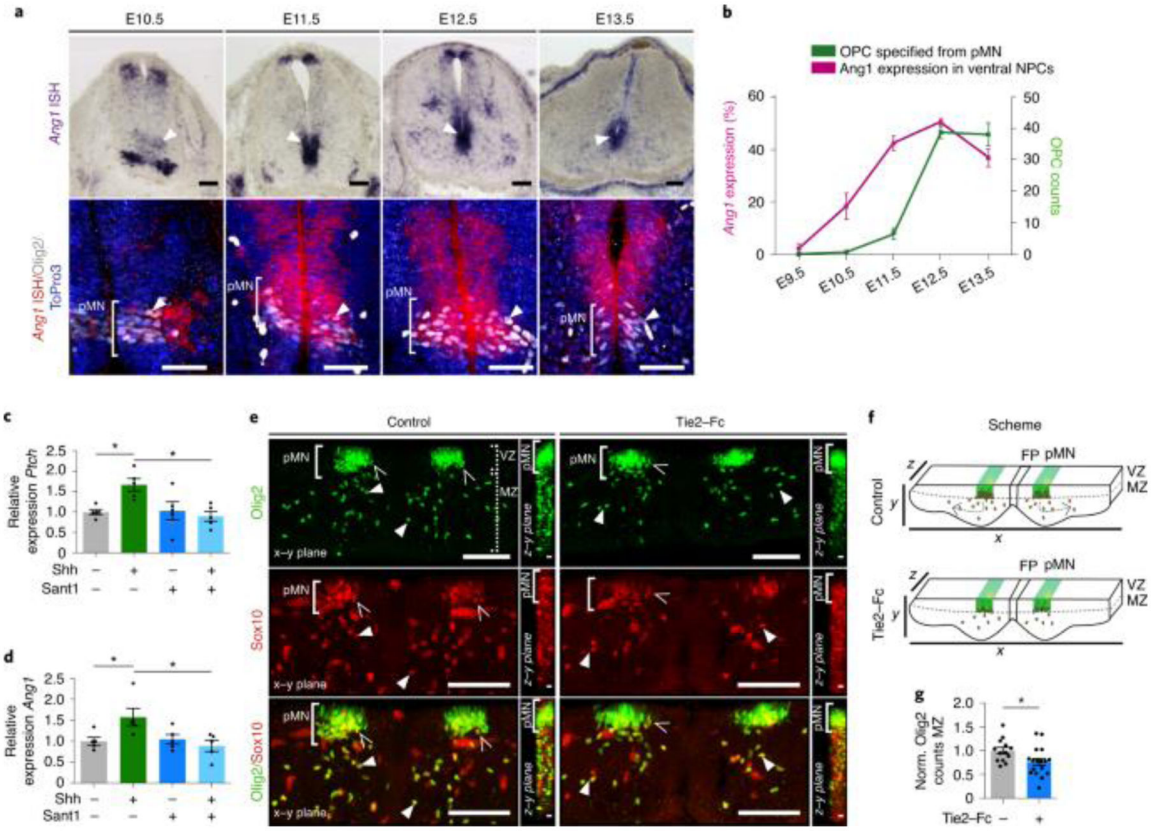

Fig. 1 |. Ang1 is expressed in SC NPCs and regulates OPC specification.

a, *Ang1* ISH in transverse sections from E10.5 to E13.5 mouse embryos at brachial level (top). Combined *Ang1* ISH (pseudo-colored in red) with Olig2 immunofluorescence (bottom). Arrowheads point to *Ang1+* co-localization with Olig2+ pMN-NpCs. Scale bar, 50 μm (bottom) and 100 μm (top). **b**, plot showing that *Ang1* expression (% of the area of *Ang1+* signal in ventral NpC domains; left *y* axis) sequentially overlaps with OpC specification (OpC counts; right *y* axis) at the pMN between E9.5 and E13.5 (see Methods for more details). Graph shows mean ± s.e.m. (Olig2 counts: E9.5: $n = 5$ images from one embryo, E10.5: $n = 20$ images from three independent embryos, E11.5: $n = 16$ images from two independent embryos, E12.5: $n = 24$ images from four independent embryos, E13.5: $n = 15$ images from four independent embryos; Ang1 expression: E9.5: $n = 6$, E10.5: $n = 8$, E11.5: $n = 7$, E12.5: $n = 14$, E13.5: $n = 7$ images from two independent embryos). **c**, **d**, Relative *Ptch* (**c**) and *Ang1* (**d**) expression in NSps derived from E11.5 SC progenitors stimulated with recombinant Shh (500 ng ml^{-1}) and/or Shh inhibitor Sant1 (150 nM). Graph shows mean ± s.e.m. ($n = 5$ independent experiments; one-way ANOVA. *Ptch:* Control versus Shh $^*P = 0.0391$; Shh versus Shh+Sant1 $^*P = 0.0142$. *Ang1:* Control versus Shh $^*P = 0.0375$; Shh versus Shh+Sant1 $^*P = 0.0242$). **e**, Whole-mount SC explants immunostained for Olig2 and Sox10 to detect OpCs (arrowheads) in the VZ and MZ after culturing in control (vehicle) or recombinant Tie2–Fc (2 μg ml^{-1}) in the *y–x* plane of *Z*-stack images. On the right side of each image, an orthogonal projection is shown for the *z–y* plane of a *Z*-stack. Scale bar, 100 μm. Open arrowheads indicate OpCs in the pMN (VZ) and filled arrowheads in the MZ. **f**, Scheme summarizing the phenotype of explants treated

with recombinant Tie2–Fc or in control conditions. The *z–y–x* planes are also depicted to illustrate the positioning of the cells. A scheme of explant preparation is also provided in Extended Data Fig. 2e. **g**, Quantification of the number of OpCs in the MZ (Olig2+) of Tie2–Fc-treated explants, normalized to vehicle-treated explants. Graph shows mean ± s.e.m. (control $n = 13$, Tie2–Fc $n = 17$; 5 independent litters). Unpaired two-sided *t*-test, $*P < 0.0248$.

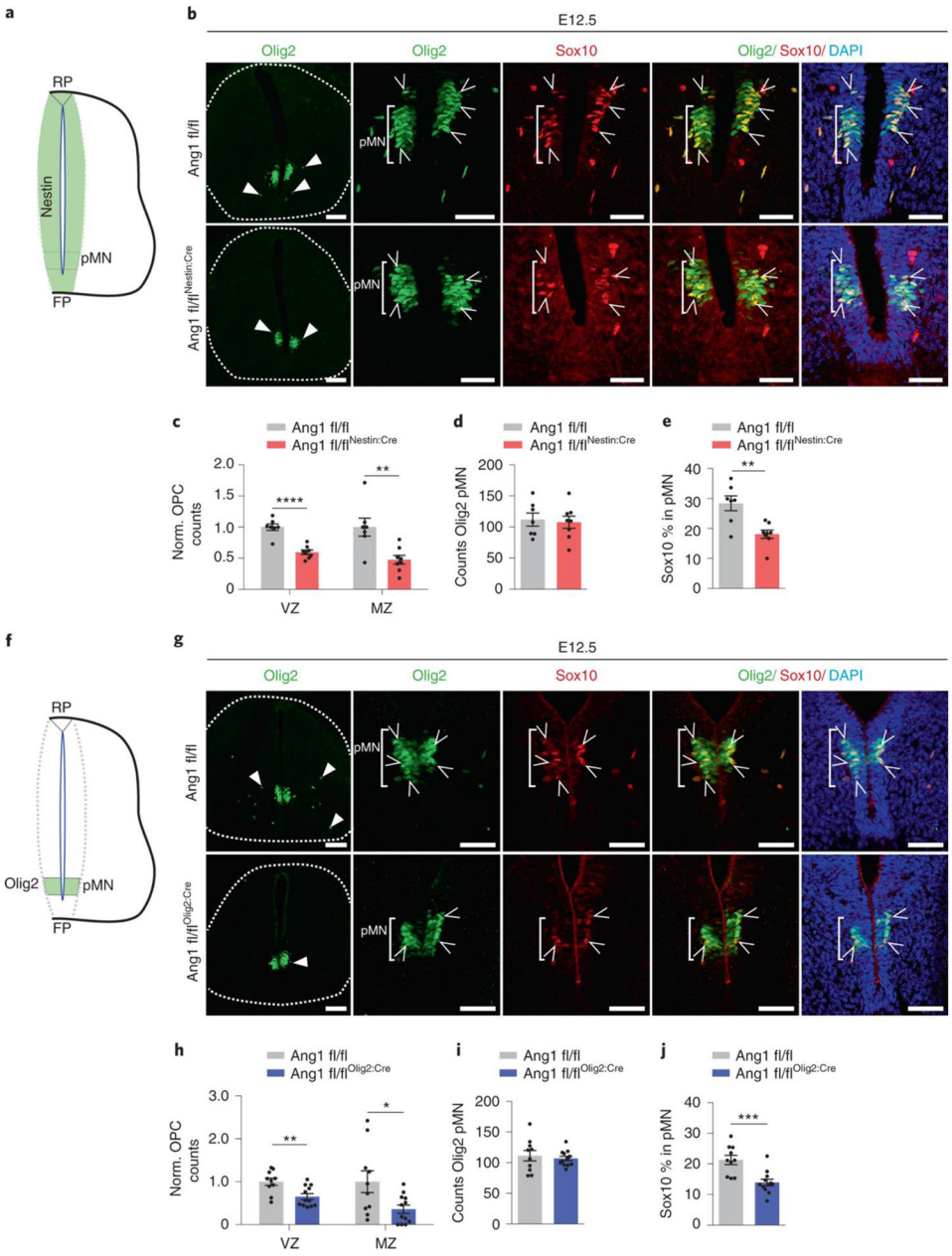

Fig. 2 |. NPC-derived Ang1 regulates OPC specification.

a, Scheme showing Nestin expression in SC NPCs to illustrate that Nestin:Cre driver mediates Ang1 deletion in all NPCs. **b**, Images of transverse sections at brachial level of Ang1 fl/fl (control) and Ang1 fl/fl$^{Nestin:Cre}$ E12.5 embryos. Left: entire SC immunostained with Olig2. Right: pMN domain immunostained for Olig2 and Sox10. Bracket, pMN; open arrowheads indicate OPCs in the pMN (VZ) and filled arrowheads in the MZ. Scale bars, 100 μm (left) and 50 μm (images of pMN). **c**, Quantification of OPCs in the VZ and MZ of Ang1 fl/fl and Ang1 fl/fl$^{Nestin:Cre}$ mice, normalized to control littermates. **d**, Analysis of the number of Olig2^{+} progenitors in the pMN. **e**, Ratio of VZ Sox10^{+} cells within the total number of Olig2^{+} pMN cells. For **c**–**e**, graphs show mean ± s.e.m. (Ang1 fl/fl $n = 7$, Ang1

fl/fl$^{Nestin:Cre}$ $n = 8$, from four independent litters). Unpaired two-sided t-test (VZ ****$P <$ 0.0001, MZ **$P = 0.0098$, Sox10% **$P = 0.0051$). **f**, Scheme showing Olig2 expression in SC pMN to illustrate that Olig2:Cre driver mediates *Ang1* deletion only in pMN and its progeny. **g**, Images of transverse sections at brachial level of Ang1 fl/fl and Ang1 fl/fl$^{Olig2:Cre}$ E12.5 embryos. Left: entire SC immunostained with Olig2. Right: pMN domain immunostained for Olig2 and Sox10. Bracket, pMN; open arrowheads indicate OPCs in the pMN and filled arrowheads in the MZ. Scale bars, 100 μm (left) and 50 μm (images of pMN). **h**, Quantification of OPCs in the VZ and MZ of Ang1 fl/fl and Ang1 fl/fl$^{Olig2:Cre}$. **i**, Analysis of the number of Olig2$^+$ progenitors in the pMN. **j**, Ratio of VZ Sox10$^+$ cells within the total number of Olig2$^+$ pMN progenitor cells. For **h**–**i**, graphs show mean ± s.e.m. (Ang1 fl/fl $n = 10$, Ang1 fl/fl$^{Olig2:Cre}$ $n = 12$, from three independent litters). Unpaired two-sided t-test (VZ **$P = 0.0050$, MZ *$P = 0.0375$, Sox10 ***$P = 0.0009$). Dashed lines mark the perimeter of the SC. FP, floor plate; RF, roof plate.

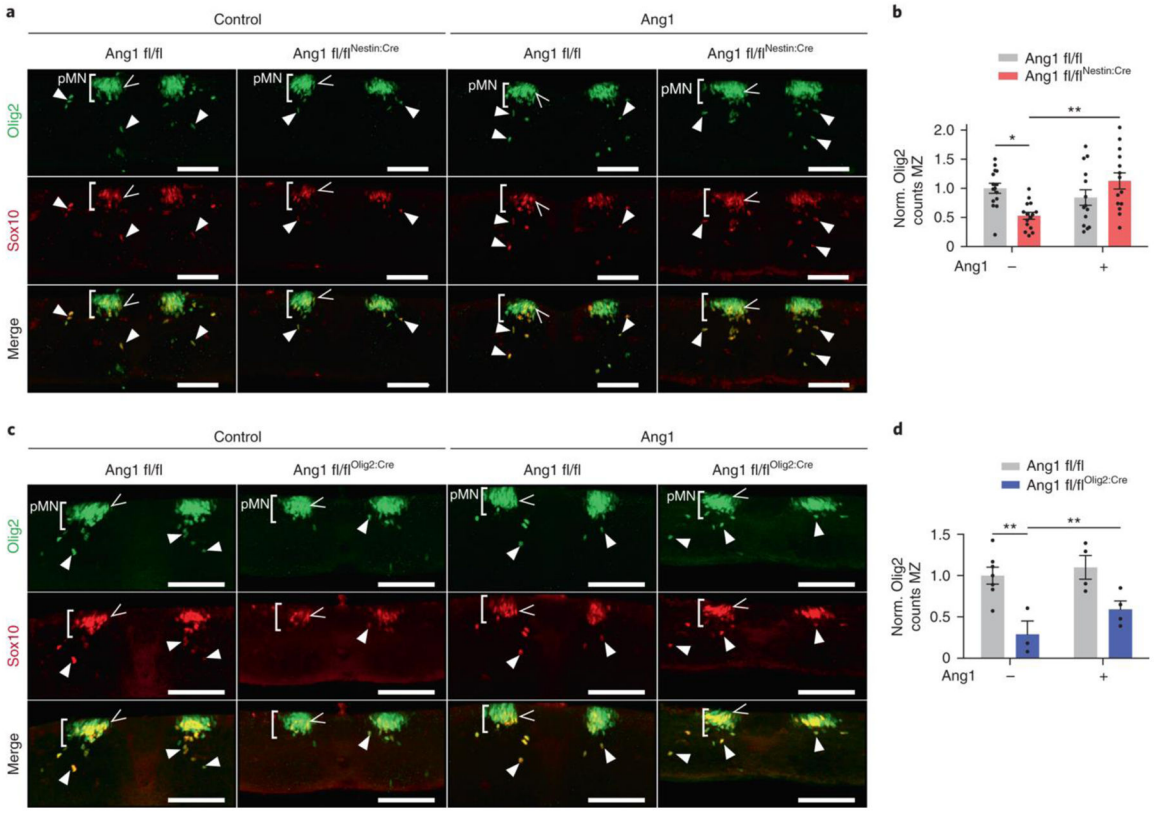

Fig. 3 |. Exogenous Ang1 rescues OPC specification defects in Ang1 fl/fl$^{Nestin:Cre}$ and Ang1 fl/fl$^{Olig2:Cre}$ embryos ex vivo.

a, 100-μm transverse sections of Ang1 fl/fl and Ang1 fl/fl$^{Nestin:Cre}$ SC explants immunostained for Olig2 and Sox10 to detect OPCs in the VZ (open arrowheads) and MZ (filled arrowheads) after culturing with control (vehicle) or recombinant Ang1 300 ng ml^{-1} for 24 h. Scale bar, 100 μm. **b**, Quantification of the number of OPCs in the MZ (Olig2^{+}), normalized to control (Ang1 fl/fl) untreated explants. Mean ± s.e.m. (Ang1 fl/fl $n = 15$ vehicle and $n = 14$ +Ang1; Ang1 fl/fl$^{Nestin:Cre}$ $n = 15$ vehicle and $n = 14$ +Ang1, from six independent litters). Two-way ANOVA (Ang1 fl/fl versus Ang1 fl/fl$^{Nestin:Cre}$ (vehicle) $*P = 0.0164$; Ang1 fl/fl$^{Nestin:Cre}$ vehicle versus Ang1 fl/fl$^{Nestin:Cre}$ +Ang1 $**P = 0.0015$). **c**, 100-μm transverse sections of Ang1 fl/fl and Ang1 fl/fl$^{Olig2:Cre}$ SC explants immunostained for Olig2 and Sox10 to detect OPCs in the VZ (open arrowheads) and MZ (filled arrowheads) after culturing with control (vehicle) or recombinant Ang1 300 ng ml^{-1} for 24 h. Scale bar, 100 μm. **d**, Quantification of the number of OPCs in the MZ (Olig2^{+}), normalized to control (Ang1 fl/fl) untreated explants. Graph shows mean ± s.e.m. (Ang1 fl/fl $n = 7$ vehicle and $n = 4$ +Ang1, Ang1 fl/fl$^{Olig2:Cre}$ $n = 3$ vehicle and $n = 4$ +Ang1, from four independent litters). Two-way ANOVA (Control Ang1 fl/fl versus Control Ang1 fl/fl$^{Olig2:Cre}$ $**P = 0.0093$; Control Ang1 fl/fl$^{Olig2:Cre}$ versus +Ang1 Ang1 fl/fl$^{Olig2:Cre}$ $**P = 0.0074$).

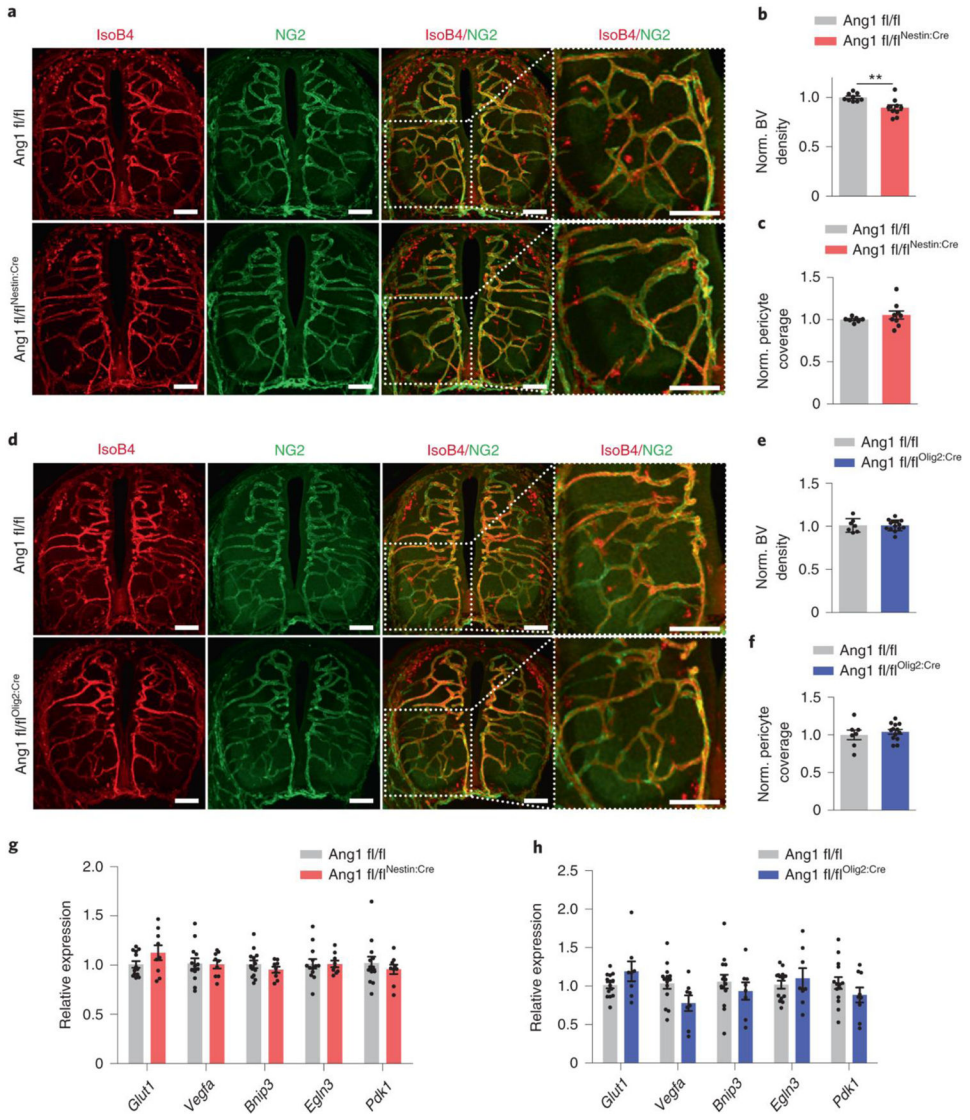

Fig. 4 |. Reduced OPC specification in Ang1-deficient embryos cannot be explained by morphological vascular defects.

a, Transverse thick sections of E12.5 Ang1 fl/fl and Ang1 fl/fl$^{Nestin:Cre}$ stained with IsoB4 to visualize blood vessels and NG2 for pericytes. Scale bar, 100 μm; inset, 50 μm. **b**, Quantification of blood vessel density in Ang1 fl/fl and Ang1 fl/fl$^{Nestin:Cre}$, normalized to control (Ang1 fl/fl) littermates. Graph shows mean ± s.e.m. (Ang1 fl/fl $n = 9$, Ang1 fl/fl$^{Nestin:Cre}$ $n = 10$, from three independent litters). Unpaired two-sided *t*-test (blood vessel density $^{**}P = 0.0041$). **c**, Quantification of pericyte coverage of blood vessels, expressed as the percentage of pericyte density with respect to the vascular density in each cross-section of Ang1 fl/fl$^{Nestin:Cre}$ and normalized to control (Ang1 fl/fl) littermates. Graph shows mean ± s.e.m. (Ang1 fl/fl $n = 9$, Ang1 fl/fl$^{Nestin:Cre}$ $n = 10$, from three independent litters). Unpaired two-sided *t*-test. **d**, Transverse thick sections of E12.5 Ang1 fl/fl (control) and Ang1 fl/fl$^{Olig2:Cre}$ stained with IsoB4 to visualize blood vessels and NG2 for pericytes. Scale bar, 100 μm; inset, 50 μm. **e**, Quantification of blood vessel density in Ang1 fl/fl and Ang1 fl/fl$^{Olig2:Cre}$, normalized to control (Ang1 fl/fl) littermates. Graph shows mean

± s.e.m. (Ang1 fl/fl $n = 7$, Ang1 fl/fl$^{Olig2:Cre}$ $n = 14$, from two independent litters). **f**, Quantification of pericyte coverage of blood vessels, expressed as the percentage of pericyte density with respect to vascular density in each cross-section of Ang1 fl/fl$^{Olig2:Cre}$ and normalized to control (Ang1 fl/fl) littermates. Graph shows mean ± s.e.m. (Ang1 fl/fl $n = 7$, Ang1 fl/fl$^{Olig2:Cre}$ $n = 13$, from two independent litters). Unpaired two-sided *t*-test. **g**, **h**, Relative expression of hypoxia response genes *Glut1*, *Vegfa*, *Bnip3*, *Egln3* and *Pdk1* from the neural compartment (CD31^{-} selection) from Ang1 fl/fl or Ang1 fl/fl$^{Nestin:Cre}$ (**g**) and Ang1 fl/fl or Ang1 fl/fl$^{Olig2:Cre}$ (**h**) E12.5 SCs. Graph shows mean ± s.e.m. (Ang1 fl/fl $n = 13$, Ang1 fl/fl$^{Nestin:Cre}$ $n = 9$, from three independent litters; Ang1 fl/fl $n = 14$, Ang1 fl/fl$^{Olig2:Cre}$ $n = 8$, from four independent litters). Unpaired two-sided *t*-test.

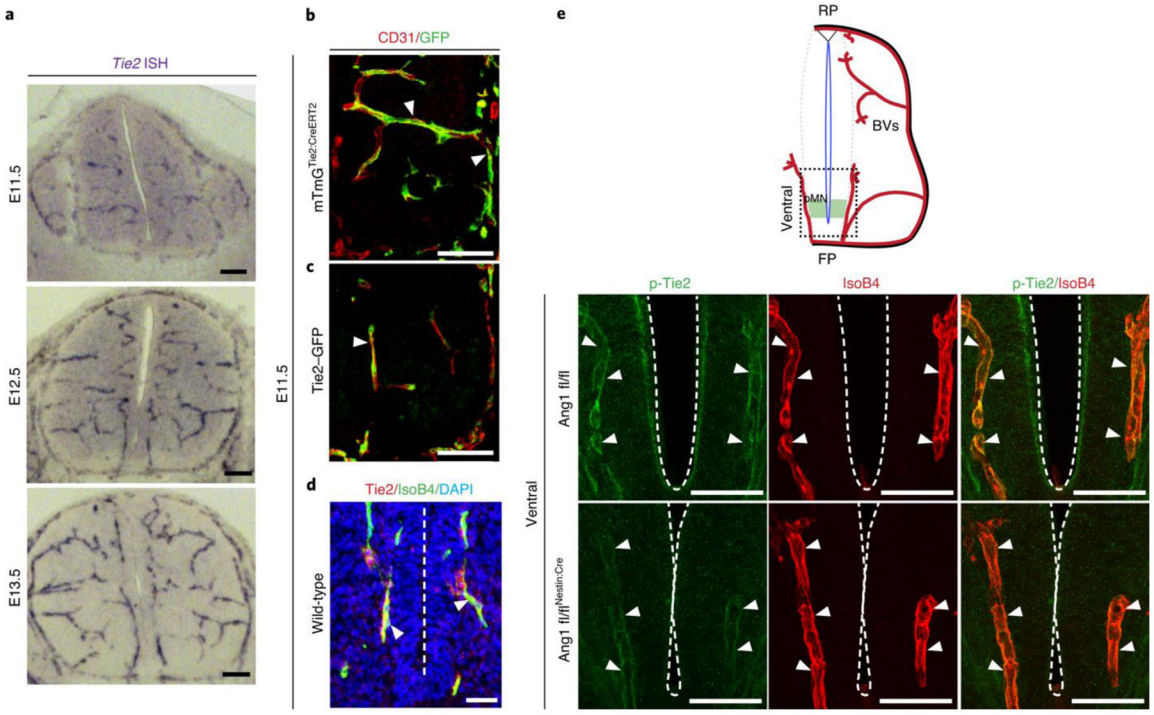

Fig. 5 |. Tie2 is exclusively expressed by blood vessels.

a, ISH for *Tie2* in transverse sections of wild-type embryos between E11.5 and E13.5. Scale bar, 100 μm. **b**, Transverse section of tamoxifen-inducible mTmG$^{Tie2:CreERT2}$ E11.5 embryo, showing Tie2-driven recombination and, consequently, GFP expression (green), co-localizing with CD31^{+} blood vessels (pseudocolored in red). Scale bar, 50 μm. **c**, Transverse section of transgenic Tie2–GFP embryo (E11.5) showing GFP (green) expression in CD31^{+} blood vessels (red). Scale bar, 50 μm. **d**, Immunofluorescence for Tie2 and IsoB4^{+} blood vessels in E11.5 wild-type embryo transverse section. Scale bar, 25 μm. **e**, Scheme of the ventral region of the SC including the pMN and adjacent blood vessels (upper panel). p-Tie2 staining combined with the blood vessel marker IsoB4 in Ang1 fl/fl$^{Nestin:Cre}$ and control littermate in blood vessels adjacent to pMN (bottom). Note the decreased Tie2 phosphorylation in vessels proximal to the VZ. Scale bar, 50 μm. All data are representative from at least three independent experiments. BV, blood vessel; FP, floor plate; RF, roof plate.

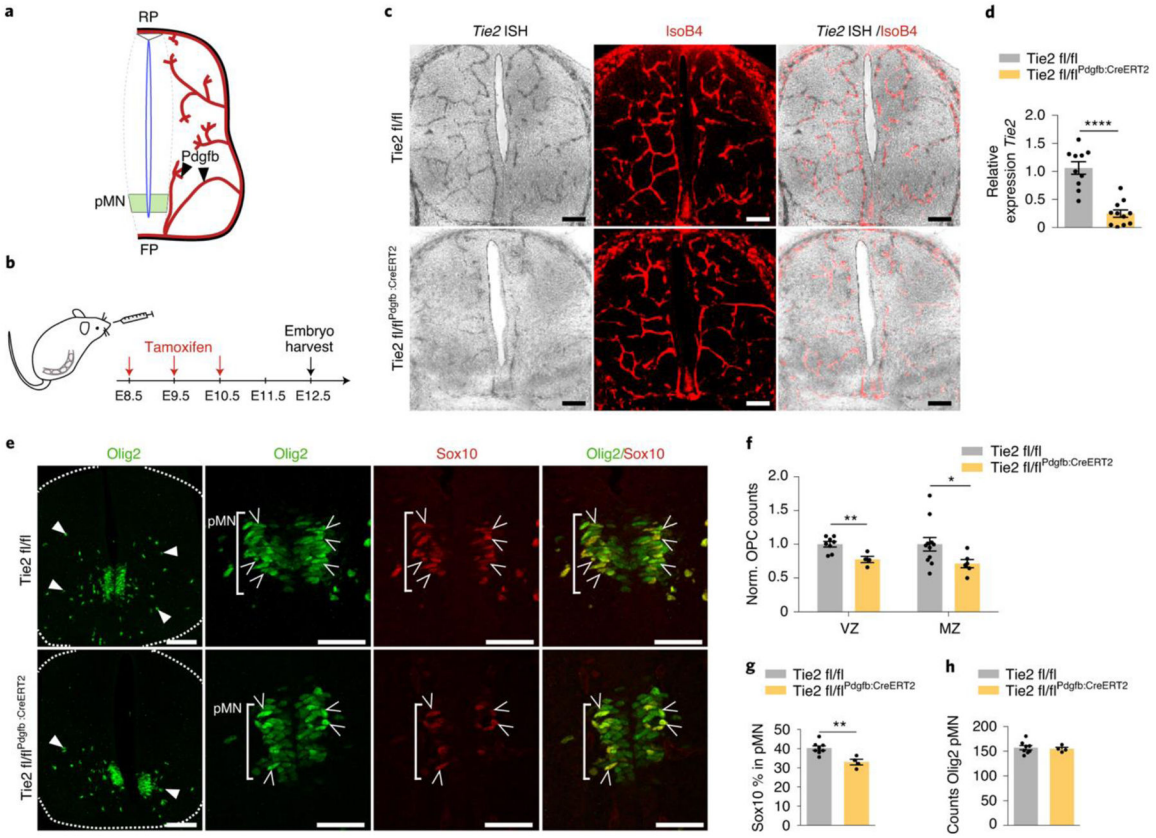

Fig. 6 |.

Z a, Schematic of Pdgfb expression in ECs of blood vessels to illustrate that Pdgfb:CreERT2 driver mediates Tie2 deletion in ECs. **b**, Protocol for tamoxifen administration to Tie2 fl/fl$^{Pdgfb:CreERT2}$ pregnant females and embryo harvest for analysis. **c**, *Tie2* ISH in E12.5 Tie2 fl/fl and Tie2 fl/fl$^{Pdgfb:CreERT2}$ embryos and combined with IsoB4 staining. Scale bar, 100 μm. **d**, Relative expression of *Tie2* mRNA in isolated ECs from E12.5 Tie2 fl/fl (control) and Tie2 fl/fl$^{Pdgfb:CreERT2}$ SCs. Graph shows mean ± s.e.m. (Tie2 fl/fl $n = 10$, Tie2 fl/fl$^{Pdgfb:CreERT2}$ $n = 11$, from three independent litters). Unpaired two-sided *t*-test (****$P < 0.0001$). **e**, Images of transverse sections at brachial level of Tie2 fl/fl and Tie2 fl/fl$^{Pdgfb:CreERT2}$ E12.5 embryos. Left: entire SC immunostained with Olig2. Right: pMN domain immunostained for Olig2 and Sox10. Bracket, pMN; open arrowheads indicate OPCs in the pMN and filled arrowheads in the MZ. Scale bars, 100 μm (left) and 50 μm (images of pMN). **f**, Quantification of OPCs in the VZ (Tie2 fl/fl $n = 8$, Tie2 fl/fl$^{Pdgfb:CreERT2}$ $n = 4$, from two independent litters) and MZ (Tie2 fl/fl $n = 11$, Tie2 fl/fl$^{Pdgfb:CreERT2}$ $n = 6$, from two independent litters) of Tie2 fl/fl and Tie2 fl/fl$^{Pdgfb:CreERT2}$, normalized to controls. **g**, Ratio of VZ Sox10$^+$ cells within the total number of Olig2$^+$ pMN progenitor cells (Tie2 fl/fl $n = 8$, Tie2 fl/fl$^{Pdgfb:CreERT2}$ $n = 4$, from two independent litters). **h**, Analysis of the number of Olig2$^+$ progenitors in the pMN (Tie2 fl/fl $n = 8$, Tie2 fl/fl$^{Pdgfb: CreERT2}$ $n = 4$, from two independent litters). Graph shows mean ± s.e.m. Unpaired two-sided *t*-test (VZ **$P = 0.0086$, MZ *$P = 0.0264$, Sox10 **$P = 0.0068$). FP, floor plate; RF, roof plate.

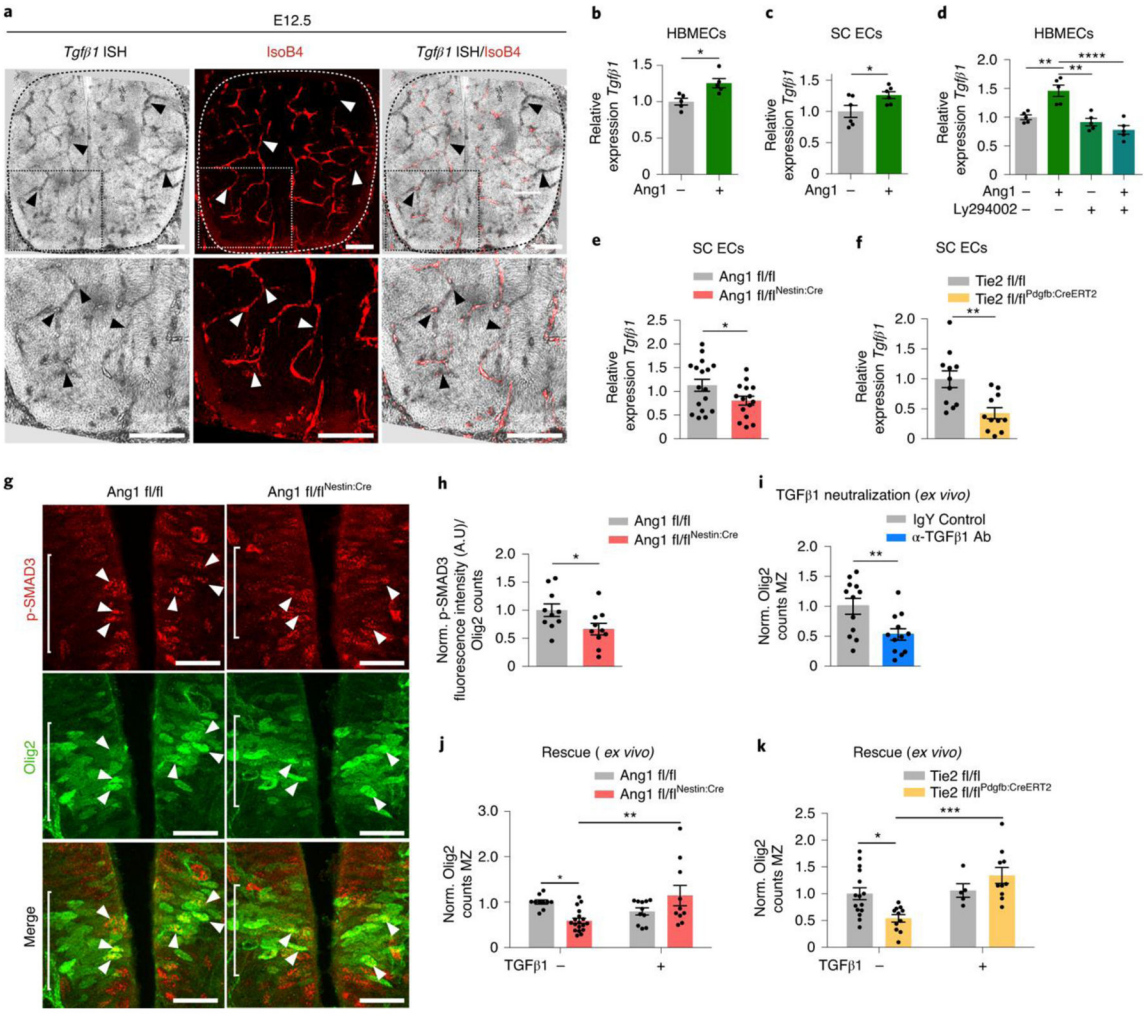

Fig. 7 |. EC-derived TGFβ1 is regulated by Tie2 signaling and required for proper OPC specification.

a, *Tgfβ1* ISH in E12.5 wild-type embryo and stained for blood vessels (IsoB4^{+}) (arrowheads show localization of *Tgfβ1* mRNA in the vasculature). Scale bar, 100 μm. **b**,**c**, Relative expression of *Tgfβ1* transcript of HBMECs (**b**) and isolated E12.5 wild-type SC ECs (**c**) upon control or recombinant Ang1 stimulation. Graphs show mean ± s.e.m. (**b**) $n = 5$ independent experiments, unpaired two-sided *t*-test $^{*}P = 0.0146$; (**c**) $n = 6$ independent experiments, unpaired two-sided *t*-test $^{*}P = 0.0479$). **d**, Relative expression of *Tgfβ1* transcript in HBMECs treated with vehicle (DMSO), recombinant Ang1 and/or Akt/PI3K inhibitor Ly294002. Graph shows mean ± s.e.m. ($n = 5$ independent experiments). One-way ANOVA, Control versus +Ang1 $^{**}P = 0.0077$; +Ang1 versus +Ly294002 $^{**}P = 0.0012$; +Ang1 versus +Ang1+Ly294002 $^{****}P < 0.0001$. **e**,**f**, Relative expression of *Tgfβ1* mRNA in CD31^{+} ECs sorted from Ang1 fl/fl and Ang1 fl/fl$^{\text{Nestin:Cre}}$ E12.5 SCs (**e**) and Tie2 fl/fl and Tie2 fl/fl$^{\text{Pdgfb:CreERT2}}$ SCs (**f**). Graphs show mean ± s.e.m. (Ang1 fl/fl $n = 17$, Ang1 fl/fl$^{\text{Nestin:Cre}}$ $n = 15$, from four independent litters, unpaired two-sided *t*-test, $^{*}P = 0.0495$; Tie2 fl/fl $n = 11$, Tie2 fl/fl $^{\text{Pdgfb: CreERT2}}$ $n = 11$, from three independent litters, unpaired two-sided *t*-test, $^{**}P = 0.0033$). **g**, Co-immunostaining for phospho-SMAD3 (p-SMAD3)

and Olig2 at the pMN level of E12.5 Ang1 fl/fl and Ang1 fl/fl$^{Nestin:Cre}$ embryo transverse section. Arrowheads show Olig2^{+}pSMAD3^{+} double-positive cells. Scale bar, 25 μm. **h**, Quantification of p-SMAD3 fluorescence intensity per Olig2^{+} cell counts in the pMN of Ang1 fl/fl and Ang1 fl/fl$^{Nestin:Cre}$ normalized to control littermates. Graph shows mean ± s.e.m. (Ang1 fl/fl $n = 10$, Ang1 fl/fl$^{Nestin:Cre}$ $n = 10$, from three independent litters). Unpaired two-sided t-test, $*P = 0.040$. AU, arbitrary units. **i**, Quantification of the number of OPCs in the MZ (Olig2^{+}) from wild-type E11.5 explants treated with α-TGFβ1 blocking antibody (α-TGFβ1 Ab) or vehicle (IgY control) (5 μg ml^{-1}) for 24 h; values are normalized to control-treated explants. Graph shows mean ± s.e.m. (IgY control $n = 12$, α-TGFβ1 Ab $n = 12$, from three independent litters). Unpaired two-sided t-test, $**P = 0.0088$. **j**, Quantification of OPC number in the MZ (Olig2^{+}) of Ang1 fl/fl and Ang1 fl/fl$^{Nestin:Cre}$ SC explants after culturing with control (vehicle) or recombinant TGFβ1 50 ng ml^{-1}, normalized to control (vehicle of Ang1 fl/fl). Graph shows mean ± s.e.m. (Ang1 fl/fl $n =$ 10 vehicle and +TGFβ1 $n = 11$; Ang1 fl/fl$^{Nestin:Cre}$ $n = 18$ vehicle and +TGFβ1 $n = 10$, from seven independent litters). Two-way ANOVA; Control Ang1 fl/fl versus Control Ang1 fl/fl$^{Nestin:Cre}$ $*P = 0.0449$; Control Ang1 fl/fl$^{Nestin:Cre}$ versus +TGFβ1 Ang1 fl/fl$^{Nestin:Cre}$ $**P = 0.0029$. **k**, Quantification of the number of OPCs in the MZ (Olig2^{+}) of Tie2 fl/fl and Tie2 fl/fl$^{Pdgfb:CreERT2}$ SC explants after culturing with control (vehicle) or recombinant TGFβ1 50 ng ml^{-1}, normalized to control (vehicle of Tie2 fl/fl). Graph shows mean ± s.e.m. (Tie2 fl/fl $n = 15$ vehicle and +TGFβ1 $n = 5$; Tie2 fl/fl $^{Pdgfb:CreERT2}$ $n = 11$ vehicle and +TGFβ1 $n = 10$, from five independent litters). Two-way ANOVA; Control Tie2 fl/fl versus Control Tie2 fl/fl $^{Pdgfb:CreERT2}$ $*P = 0.0278$; Control Tie2 fl/fl $^{Pdgfb:CreERT2}$ versus +TGFβ1 Tie2 fl/fl $^{Pdgfb:CreERT2}$ $***P = 0.0002$.